Li Yiran (Orcid ID: 0000-0002-5921-7496)
Levin Vadim (Orcid ID: 0000-0001-7317-4819)

# Localized Anisotropic Domains Beneath Eastern North America

**Yiran Li[1], Vadim Levin[1], Stephen Elkington[1], and Janine Hlavaty[1]**

[1]Department of Earth and Planetary Sciences, Rutgers University, Piscataway, New Jersey, USA.

Corresponding author: Yiran Li (yiran.c.li@gmail.com)

**Key Points:**

- We used a common set of earthquake sources to compile averaged and individual shear wave splitting parameters at 33 stations.
- We used multiple traits of splitting parameters observed at each site to define four anisotropic domains in eastern North America.
- Domains do not align with Appalachian geology, and likely reflect variations of olivine fabric within the lithospheric mantle.

**Abstract**

Seismic anisotropy beneath eastern North America likely reflects both the remnant lithospheric fabrics and the present-day deformation of the asthenosphere. We report new observations of splitting in core-refracted shear phases observed over 3-5 years at 33 sites in New Jersey, New York, and states in the New England region, and also include data from 8 previously studied locations. Our data set emphasizes back-azimuthal coverage necessary to capture the directional variation of splitting parameters expected from vertically varying anisotropy. We report single-phase splitting parameters as well as station-averaged values based on splitting intensity technique that incorporates all observed records regardless of whether they showed evidence of splitting or not. Trends of averaged fast shear wave polarizations appear coherent and are approximately aligned with absolute plate motion direction. The general disparity between the fast axes and the trend of surface tectonic features suggests a dominant asthenosphere contribution for the observed seismic anisotropy. Averaged delay values systematically increase from ~0.5 s in New Jersey to ~1.4 s in Maine. Splitting parameters vary at all sites, and neighboring stations often show similar patterns of directional variation. We developed criteria to group stations based on their splitting patterns and identified four domains with distinct anisotropic properties. Splitting patterns of three domains suggest a layered anisotropic structure that is geographically variable, outlining distinct regions in the continental mantle, e.g. the Proterozoic lithosphere of the Adirondack Mountains. A domain coincident with the North Appalachian Anomaly displays virtually no splitting, implying that the lithospheric fabric was locally erased.

This article has been accepted for publication and undergone full peer review but has not been through the copyediting, typesetting, pagination and proofreading process which may lead to differences between this version and the Version of Record. Please cite this article as doi: 10.1029/2019GC008518

**Plain Language Summary**
Over the course of the last 1 billion years of Earth's existence the eastern part of the North American continent was affected by repeated episodes of major tectonic change: continental collisions formed major mountain belts, while the breakup of continents led to the opening of new oceanic basins. While at present the area is devoid of major tectonic activity, the rocks making up the crust and the shallow part of the upper mantle (down to ~100 km into the Earth) likely preserve the record of past events that shaped the region in the form of a systematic fabric imposed when major deformation (compression, shear) occurred. At greater depth another fabric is expected due to the motion of tectonic plates (such as North America) and to the slow convection of the Earth's solid, but flowing interior. A systematic fabric in the rocks making up the upper 400 km of the Earth leads to the directional dependence (anisotropy) of their elastic properties, and consequently makes the speed of seismic waves from distant earthquakes directionally dependent. The nature of this directional dependence (e.g., which direction is faster) provides clues about the systematic fabric of the Earth's interior, offering a means to read the record of past deformation episodes, and to characterize the nature of the present-day ones. In this study we used records of seismic waves from numerous distant earthquakes observed at a set of seismographs in eastern North America to create a detailed description of the attributes of directionally dependent speed of seismic waves. We took care to create mutually compatible sets of records for all sites we have examined and developed a set of criteria that allowed us to group our observations into "domains" – areas where the nature of directional dependence of seismic speed was similar, and distinct from other parts of the region.
The shapes of the domains we have outlined provide clues to the interior configuration of the North American tectonic plate and will help in future studies of its correct state and past history. One domain corresponds to the area of the Adirondack Mountains in upstate New York – a region where a major elevated plateau existed ~1 b. y. ago, and where little has happened since. Another domain appears to be related to an area of previously proposed ongoing upwelling (upward flow) of warm material beneath New England. Our results are of interest for reading the record of past activity in the region we have studied, and more generally as an example of how to probe Earth's interior structure in high detail.

## 1 Introduction

The surface geology of eastern North America records two complete Wilson Cycles that have shaped its lithosphere for more than a billion years. From the assembly of supercontinent Rodinia by ~1.0 Ga to the formation of present-day passive margin flanking the Atlantic Ocean, the region has transitioned through a series of tectonic regimes, including rifting, subduction, and orogenesis (e.g. Hatcher, 2010; Hynes & Rivers, 2010; Thomas, 2006). The continental breakup and assimilation of foreign landmasses require plate-scale deformation that has likely left remnant structures within the now-stable continental lithosphere. The detailed characterization of seismic anisotropy provides useful insights for inferring the strength and the scale of deformed structures at depth. Recently, increased station density and duration of data collection has enabled the characterization of finer scale lateral variation of the seismic properties. The improved lateral resolution illuminates potentially ongoing modification of the upper mantle rocks by local geodynamic processes, introducing additional complexities and details to the existing interpretations of seismic anisotropy in the region.

Seismic anisotropy is the dependence of seismic velocity on directionally varying elastic properties. Anisotropic structures within the Earth's upper mantle are commonly associated with the strain-induced alignment of anisotropic minerals (e.g. Nicolas & Christensen, 1987; Zhang & Karato, 1995), particularly of olivine. The ductile deformation due to plate motion and mantle convection thus produces pervasive mineralogical fabrics that can be detected and characterized using seismic waves that are sensitive to the effects of anisotropy (e.g., Long & Becker, 2010). Additionally, the fabrics of past deformation preserved within the rigid lithospheric mantle, if substantial in strength and spatial dimensions, may also add their

signature to the observed effects of anisotropy. In eastern North America, the history of accretion of distinct lithospheric mantle fragments belonging to Gondwana-derived tectonic terranes (Figure 1) makes the contribution of the fossil fabrics likely. Conversely, the modification of the lithosphere following the orogeny (e.g. by an episode of delamination) may involve processes that overprint the signatures of fossil fabrics.

Shear wave splitting is a widely used technique to characterize the upper mantle anisotropy. Early studies (e.g. Barruol et al., 1997; Levin et al., 1999, 2000; Silver & Chan, 1988; Vinnik et al., 1989) confirmed the presence and the pervasiveness of seismic anisotropy in the upper mantle of eastern North America. The specific attributes of anisotropy within the upper mantle of the region, and whether it resides in the asthenosphere or the lithosphere, are a matter of ongoing research (e.g. Long et al., 2015; White-gaynor & Nyblade, 2017). Relative contributions from different source regions are commonly assessed on the basis of uniformity in the observed parameters across a region. An alignment of anisotropic directions with surface tectonic features is often cited as the evidence for a strong lithospheric contribution to the inferred anisotropy (e.g. Gilligan et al., 2016). In eastern North America, studies by Levin et al. (1999, 2000) and Yuan and Levin (2014) proposed a regionally uniform set of anisotropic layers to explain the apparent similarity of directional variation in shear wave splitting at observing locations separated by hundreds of kilometers.

Improved station spacing following the deployment of the EarthScope Transportable Array (IRIS Transportable Array, 2003) made it possible to refine the definition of anisotropic properties in eastern North America. Regional compilation of shear wave splitting observations by Long et al. (2015) and Yang et al. (2017) identified broad geographical differences in splitting parameters. Further characterization of strong localized variation was enabled by the use of long-running stations in the study by Levin et al. (2018). The improved directional coverage due to an extended period of data collection enabled a more complete sampling of the pattern and consequently more detailed characterization of the underlying anisotropy. Notable differences in the observed patterns of shear wave splitting seen at proximal stations offered evidence for potentially finer and sharper lateral variations within regions that were previously assumed to be homogenous.

In this study, we present a systematic survey of long-running sites with an aim of combining the ability to see the lateral variations with the directional dependence of splitting that was previously taken to signify layering of anisotropic properties. A similar approach has been adopted by Chen et al. (2018) and Levin et al. (2018) to discern potential areas of unique anisotropic properties based on the specific behaviors of directional variation within the dataset of an individual station. We extend this mode of characterization to a broader region to examine the finer-scale lateral variations in detail.

## 2 Methodology and Data

In an anisotropic medium, a shear wave splits into two orthogonal quasi-shear waves that travel with different velocities (Savage, 1999; Silver & Chan, 1991; Vinnik et al., 1989). For conditions within the sub-lithospheric upper mantle, the fast wave is expected to orient sub-parallel to the direction of maximum deformation (Crampin, 1977; Long & Silver, 2009; Park & Levin, 2002). In addition, a delay accumulates between the arrivals of fast and slow quasi-shear waves in proportion to the strength of anisotropy, as well as to the length of the path which the wave takes to travel through the anisotropic media. The orientation of the fast polarization and the delay time between the two waves can be estimated using the three-

component seismograms and are thus conventionally used as parameters that describe the effects of anisotropy on the shear waves (e.g.; Bowman & Ando, 1987; Silver & Chan, 1991).

The splitting of core-refracted shear phases is commonly used to probe upper mantle anisotropy because of the relative ease of attributing their splitting parameters (Long & Silver 2009; Vinnik et al., 1989). Specifically, the phases lose all source-side influence due to their paths through the liquid outer core, and assume a predictable polarization after propagating through the core-mantle boundary (e.g. Savage, 1999; Silver, 1996). More importantly, the steep incidence of core-refracted phases provides good lateral resolution that is beneficial for examining the spatial variation of splitting patterns (Alsina & Snieder, 1995; Long & Silver 2009). The comparisons with other geological observations are often done using pairs of averaged splitting parameters (delay times and fast polarizations) from individual stations (e.g. Long et al., 2015; Yang et al., 2017). While this approach allows associations with broad regional patterns, it may overlook the variations within the datasets of individual stations that potentially reflect the complexity in anisotropic structures (Levin et al., 1999). We attempt to extract more details by comparing sets of individual splitting parameters at each station and assessing the degree of similarity between them.

We selected 33 stations (Figure 1) from combined networks of permanent observatories (New England Seismic Networks (Albuquerque Seismological Laboratory (ASL)/USG, 1994); POLARIS Networks, https://ds.iris.edu/mda/PO; United States National Seismic Network (Albuquerque Seismological Laboratory (ASL)/USGS 1990); Canadian National Seismograph Network (Geological Survey of Canada, 1989); Lamont-Doherty Cooperative Seismic Network, https://ds.iris.edu/mda/LD), and Central and Eastern US Network (UC San Diego, 2013) that has retained a subset of USArray Transportable Array (IRIS Transportable Array, 2003) sites for long-term operation. The extended duration of data retrieval (3 – 5 years) was necessary to optimize back azimuthal coverage of the seismic sources and observe the systematic variations of the splitting parameters. The estimated inter-station spacing as small as ~30 km in parts of the region allows us to characterize relatively abrupt lateral variations in splitting parameters that may be attributed to small-scale structures within the upper mantle.

We measured all core-refracted phases that were visible in our records, including SKS, SKKS, and PKS phases (called XKS hereafter). To effectively compare splitting behaviors between stations, we created a template list of seismic sources using a continuous permanent station (NE.PQI, Figure 1). We selected the sources according to specific thresholds for magnitudes and epicentral distances (Mw. 6.0, and epicentral distances between 85° and 140°) to ensure the visibility of core-refracted phases. The relevant events that occurred between years 2013 and 2017 were then further inspected for clarity of signals. The resulting template consists of 61 visible events with optimal back azimuthal coverage (Figure 3d). The lack of events from the east may be attributed to the lack of convergent margins in the respective direction. For each station, we systematically retrieved the seismograms according to the event list to reduce the uncertainty introduced by source effects when comparing the individual splitting parameters. To further minimize bias and ensure systematic data collection, we randomly assigned stations to three analysts and measured in bulk using the SplitLab software (Wüstefeld et al., 2008).

For each record, we first examined the signals in both LQT (ray-based) and ZEN (vertical-east-north) coordinate systems to gauge suitable bandpass filter limits for smoothing the waveforms. The filters were manually adjusted for individual measurements, except for a

number of exceptionally clear waveforms for which the filters were not needed. The lower limits were mostly between 0.01 and 0.03 Hz, and the upper limits ranged anywhere between 0.04 and 1.50 Hz. The waveform in the transverse component of the LQT system was assessed in particular for obvious absence of signal that may immediately suggest non-split (NULL) measurements (Figure 2a). For most cases, we determined measurement types and splitting parameters after reviewing complementary observables provided by SplitLab, including particle motions, the transverse waveforms before and after correction for anisotropic effects, and the characteristic discrepancy of splitting parameters between different measurement techniques.

We chose to interpret splitting parameters quantified by the Rotation-Correlation (RC) method (Bowman & Ando, 1987) to be consistent with previous studies by Levin et al. (1999; 2000; 2018). In our experience this technique produces intuitively small delay times for the cases of NULL measurements. For complex anisotropic structures and high noise levels the method is known to yield fast axes that are systematically 45° away from the incident ray back azimuth (Wüstefeld & Bokelmann, 2007). However, the extent and patterns to which the splitting parameters fluctuate with respect to the back azimuth appear to change depending on how the underlying anisotropy varies with depth. We utilized splitting parameters obtained by the minimization of the transverse component method (Silver and Chan, 1991; SC hereafter) as supplementary information. We often found the values from RC and SC techniques to be different for the same set of records. The consistency or discrepancy of the resulting parameters between the RC and the SC methods were noted for assessing the quality of our measurements. However, given the careful quality control performed prior to data analysis and the commitment to retain the desired back azimuthal coverage, we interpreted the discrepant splitting parameters to be a consequence of complex anisotropic structures (e.g. Long & van der Hilst, 2005; Wüstefeld & Bokelmann, 2007) and retained all measured results. The rectilinear particle motion (Figure 2b), and the exceptionally small delay time yielded by the RC method coupled with the exceptionally large delay time (reaching the maximum value assigned for grid search) yielded by the SC method were the key determinants for NULL measurements. Conversely, the presence of signals in the transverse component, as well as the elliptical particle motion (Figure 3b) were noted for split measurements. We saved the results after examining the persistence of characteristic observations and stability of parameter values with different time windows selections and filters. Additional details on the procedure employed to assess the measurement type (split or non-split) and quality closely follows the methodology described in Chen et al., (2018).

In addition to estimating splitting in individual XKS records we have also obtained pairs of best-fit splitting parameters for each station using the multichannel approach proposed by Chevrot (2000). This method ensures the incorporation of observations deemed to be NULL in the estimate. The method utilizes a sinusoidal pattern of splitting intensity values (SI) expected as the function of varying back azimuths and delay times, described by the relationship;

$$SI = \delta t \times \sin [2(\varphi_o - \varphi)],$$

where $\delta t$ is the best-fit delay time, $\varphi$ is the best-fit fast axis polarization, $\varphi_o$ is the back azimuth, and SI is the measure of the similarity between the transverse signal and the time derivative of the radial signal (Chevrot, 2000). To obtain SI measurements for individual XKS records we adopted a modified version of SplitLab developed by Deng et al. (2017). All measured SI values from each station were collectively fitted to a sinusoid by a least square

minimization method, from which the splitting parameters (delay times and fast polarizations) for a single layer of anisotropy were derived using the formula above (Figure 2d). We defined the uncertainties for both splitting parameters as the highest and the lowest values that fell within 95% confidence interval of the mean. To verify the reliability of the multichannel method, we also computed arithmetic means of individual delay times and fast polarization orientations for all split measurements obtained for each station. The standard deviations were defined as the uncertainty for the arithmetic means. The two sets of splitting parameters, the averages and the SI best-fit pairs, and the directional variations of individual splitting parameters at each station (Figure 2c), form the dataset that we will characterize and interpret in the subsequent sections.

All measurements and averages are compiled in supplementary tables S2 and S3, and also illustrated in Supplementary figures S1 through S33.

## 3 Results

In total, we have accumulated 1393 pairs of new splitting parameters from 33 stations in the Northeastern Appalachians and the adjacent Grenville Province. Of those, 500 pairs were deemed NULL based on the criteria described in the Methodology and Data section. Although we strived for the clarity of waveforms and the uniformity of events measured at each station, about 30% of the total expected records were culled due to excessive noise or instrument malfunction. In the end, the number of measurements per station ranges between 19 and 78, with 20 of the stations having more than 35 measurements.

Figure 3 shows examples of good single-event splitting parameters captured by nearly all of the stations. Generally, the splitting parameters yielded by a single event show regionally coherent fast polarization. While the delay times are laterally variable, the patterns in which the delay times vary over the study area are remarkably similar for events with similar NE event back azimuths (Figure 3a, 3b). In particular, the largest delay times and SI values concentrate in northern Maine and northern New York. Elsewhere, the measurements show relatively small delay times or were ranked as NULL observations and are accompanied by correspondingly small SI values. The overall fast polarization and SI values, and the spatial variation of delay times changes dramatically when the same region is sampled by waves propagating from NW (Figure 3c). Fast polarizations shift to orient dominantly WNW-ESE, and largest delay times are instead recorded in southern Canada and southern Maine. All stations thus show evidence for directional variation of splitting parameters.

In order to characterize the splitting patterns with optimal station density, we incorporated the stations from previous affiliated studies that followed similar procedures of data retrieval and classification. Namely, we included data from stations PQI and GGN featured in Li et al. (2017) and six stations (PKME, HNH, MCVT, NCB, QUA2, and UCCT) analyzed in Levin et al. (2018). Our combined data set includes 41 locations and includes over 2000 XKS phase observations. We describe both the regional patterns of station-averaged splitting parameters, as well as the localized regions of distinct splitting patterns defined through qualitative and quantitative examinations of splitting parameters within each station.

### 3.1 Regional Trends of Station-Averaged Splitting Parameters

Figure 4 shows two pairs of averaged splitting parameters at each station. Fast polarization directions obtained by fitting SI measurements show regionally coherent orientations, with values ranging between azimuths of 69° and 96° (Figure 5a). While the dominant orientation

approaches the arithmetic mean with smaller number of bins, it generally remains between the range of 70° and 80° azimuths. Values obtained by fitting SI measurements are very similar to the values obtained by the simple averages of splitting measurements, which only consider the measurements that were deemed split (Figure 5b). While the peak resides in the same range as that for the distribution yielded by SI best fit values, the distribution of simple averages appears to be wider, ranging between 61° and 106° azimuths, and more symmetrical.

Both methods of obtaining a single fast polarization for a station result in distributions with peaks that lie consistently clockwise from the region's absolute plate motion direction (approximately 249° azimuth) predicted by HS3-NUVEL1A model based on a hot spot reference frame (Gripp & Gordon, 2002). This systematic mismatch between the absolute plate motion direction and the dominant fast polarization orientation is further reinforced by the observation of NULL (non-split) measurements (Figure 5c). Generally, waves coming from the back azimuthal range in alignment with the fast polarization orientation within the anisotropic media are expected to yield NULL measurements (e.g. Savage, 1999). In the range of back azimuths sampled by our observations, NULL measurements concentrate in a WSW orientation, with a dominant peak appearing between 260° and 270° azimuths (80° to 90° azimuth in modulo 180°). Again, the dominant NULL-yielding back azimuthal range is in better agreement with the mean station-averaged fast polarization orientations than the regional direction of the absolute plate motion. Under the assumption of a single layer of anisotropy with a horizontal symmetry axis, our results would require the orientation of the axis to be systematically different from that of the APM.

The associations between the fast polarizations and the trends of the Appalachian tectonic features and topography are unclear. Peaks in the distributions of fast polarizations obtained with both methods are well out of the range for the orientation of the orogenic trend, which rotates clockwise from about 10° azimuth in the southern part to approximately 40° azimuth in the northern part of our study area (Figure 1). Noteworthy though, is the presence of some NULL measurements falling within the range of back azimuth in alignment with the above orientation of orogenic trend.

The average delay times are laterally variable with a discernable regional trend evident in both sets of values – averages and results of fitting the SI measurements (Figure 6a). Both sets of delay time distributions show an increase from the average of ~0.5 s at the southern end to the maximum of nearly 1.4 s at the northern end of our study area (Figure 6a). Small local anomalies are also present, as evidenced by the abrupt reduction of delay times near the latitudes 42°N and 44°N, more clearly captured by the values obtained with the SI technique (Figure 6b) and to a lesser extent by results of averaging splitting delays (Figure 6c). These locations correspond to the splitting parameters from stations L64A and HNH respectively (Figure 4), which are distinguished by the high proportions of NULL measurements observed from all sampled back azimuths.

The lateral variation of delay times manifests differently between the two averaging techniques. As with the case of fast axes orientations, delay times obtained by the simple averages show relatively smooth, unimodal distribution (Figure 7b). While stations in the south (40° to 44° latitude) show smaller uncertainties than those in the north (44° to 48° latitude), the regional trend of delay times captured by simple averaging is best described as a gradual increase from the south to the north, due to the large error bars and the significant overlap between adjacent stations (Figure 6c). In contrast, values obtained from the SI

technique (Figure 7a) show a wider spread of delay times, ranging from values as small as 0.1 s obtained at stations like L64A and HNH, to as large as 1.38 s obtained at station G65A in northern Maine. While one peak forms near the arithmetic mean of about 0.76 seconds, the distribution is hardly unimodal, but better characterized as having multiple peaks at different delay times (Figure 7a). Such distribution obtained by the SI technique suggests that lateral variation of delay times may be spatially discrete. The regional trend of delay times obtained by the SI technique (Figure 6b) is also consistent with this view. Uncertainties of delay times derived by fitting SI measurements, as reported by the least squares fitting algorithm, are much smaller than those obtained by simple averaging. As a result, the regional variation in SI-derived delay values suggests two different populations of delay times, in addition to the sharp local reduction delay times at stations like HNH and L64A. Specifically, the stations in the latitude range of 40° to 43° collectively show smaller delay times (average of 0.7 second) than those in the latitude range of 44° to 48° (average of 1.0 second).

### 3.2 Regional Characterization of Directional Patterns in Splitting Parameters.

Directional variation of splitting parameters (fast polarizations and delays) reflects complexity of anisotropic structure at depth (Levin et al., 1999; Savage, 1999; Silver & Savage 1994), arising from either vertical or lateral changes in attributes (direction, strength) of anisotropy. Standard methods of estimating splitting parameters assume a single layer of horizontal-axis anisotropy. When anisotropy is complex, values of individual splitting measurements are a function of ray and symmetry axis orientations. Furthermore, different measurement algorithms are likely to yield divergent results for the same data when complexity of the underlying anisotropy and/or the level of noise in the data are high (Wüstefeld & Bokelmann, 2007).

All stations in our study show variation of individual splitting parameters that is dependent on the back azimuths and the incidence angles of the phases. Furthermore, we note that the patterns of variation at individual stations captured by the overall appearance of the directional dependence diagrams (the stereonets, e.g. Figure 8) are clearly distinct.

By visually comparing the appearance of splitting patterns in stereonets (Figure 8 and Supplementary figures S1 to S33), we find that neighboring stations generally share similar splitting characteristics. We group our 41 stations into four anisotropic domains based on a combination of qualitative and quantitative traits, and a reasonable geographical proximity. The specific criteria used are:

1) the fraction of NULL measurements in the dataset of an individual station,
2) the back azimuthal distribution of NULL measurements (dispersed vs. concentrated),
3) the variation of individual fast polarization orientations and delay times with respect to back azimuth and incidence angle, and
4) the fast polarization orientations and delay times derived by fitting SI values.

Because we used a homogenized set of earthquake sources, obtained each XKS splitting measurement through a predefined procedure (see Methodology and Data section), and because individual sites were randomly assigned to different analysts, we regard the differences in splitting patterns as reflective of truly distinct anisotropic structures at depth. Characteristics of each anisotropic domain are described in the following section. Domains are named with arbitrary color codes and were defined purely on the basis of observed shear wave splitting patterns and values. Spatial correlations of domain boundaries with other

observables, such as the surface tectonic features and the distribution of seismic velocities at depth, are addressed in the Discussion section.

### 3.2.1. Description of Anisotropic Domains

In this section we provide a detailed description of traits that we used to define the boundaries of individual domains in Figure 8. Representative stereonet diagrams are shown in Figure 8, and diagrams for each site are presented in an electronic supplement, Figures S1 to S33. A concise summary of the descriptions is also compiled in the supplement Table S1.

#### *3.2.1.1. Yellow*

The most distinct within our study region is the yellow domain. Represented by the observations from stations such as L64A and HNH, it is characterized by the high proportion of NULL measurements within the datasets of individual stations (Figure 9a). Compared to the regional average of about 35% of individual splitting parameters being NULL, stations enclosed by the yellow domain have NULL proportions up to a maximum of 83%. The strong variation of fast polarization orientations, evidenced by large (up to 42°) standard deviations (Figure 9b), may be attributed to the sampling bias due to the low number of split measurements. However, the split measurements appear remarkably similar between the stations when the NULL measurements are removed. The significantly small standard deviation for the delay times (Figure 9c) may also be attributed to the same sampling bias. Although the fraction of NULLs decreases at locations close to the boundaries of the yellow domain, averaged delay times at these sites remains small compared to the surrounding stations. The boundary between the yellow domain and the adjacent green and blue domains is drawn to include all locations that exhibit the sharp contrast of the delay times and the relatively high NULL fractions.

#### *3.2.1.2. Red*

The red domain, southwest from the yellow domain, encompasses the locality of second smallest averaged delay times. The fraction of NULL measurements within this domain is about 39%, slightly higher than the regional average. The highest site-specific NULL fraction within this domain is 53%, a value that is within the range of NULL proportions observed in the yellow domain. Additionally, the back azimuthal distributions of the NULL measurements are less dispersed, with a discernable dominant NULL direction from WNW, as well as clusters of NULL measurements from the North and the South. The red domain is distinguished from the green domain to its north by the higher proportion of NULLs (Figure 9a), as well as the degree to which the individual splitting parameters vary with respect to the incident back azimuths. Specifically, the delay times within red domain remain relatively constant with respect to the incident back azimuths, as evidenced by their small standard deviations (Figure 9c). The fast polarizations vary moderately, as evidenced by their large standard deviation values (Figure 9b). Also, fast directions within this domain have a distinct bimodal distribution of the individual fast axes (e.g.; Figures S2c, S27c, S29c).

#### *3.2.1.3. Green*

The stations in the green domain collectively have lower numbers of NULL measurements compared to the domains further south (Figure 9a; Supplementary Table 1). They are most distinguished by the concentration of NULL measurements from WNW (Figures S1a, S16a,

S17a, S28a), as well as the limited range of fast polarization directions, as evidenced by the smaller standard deviation relative to the surrounding domains (Figure 9b). The delay times, on the other hand, show a stronger level of variation relative to the more southern domains (Figure 9c). Qualitatively, most stations grouped into the green domain show systematically larger delay times in the northeastern quadrant, and smaller ones in the northwestern quadrant (Figure 8a). Ranges over which fast polarizations and delay times vary at individual sites of this domain are very similar, suggesting relatively homogenous anisotropic structure. Systematic variation in fast polarizations that is very similar at all sites is consistent with the vertical layering of anisotropy beneath this domain. The consistency of splitting patterns between different stations is in part supported by the relatively similar values of standard deviations within the green domain for both the fast axes orientations and the delay times.

*3.2.1.4. Blue*

The blue domain contains the most diverse splitting patterns, for both station-averaged and individual parameters. Though it shares similarities with the red and green domains, the blue domain is distinct for possessing strong variations for both the fast polarizations and the delay times, while the other two domains are characterized by having one parameter fluctuating more strongly than the other. Collectively, the individual fast polarizations in the blue domain form a bimodal distribution in the histogram (e.g.; Figures S6c, S7c, S13c, S14c), and the delay times encompass a large range. The most prominent examples of such qualities can be observed in the northern Maine (stations F63A and G62A, Figure 1). The splitting patterns are variable from the center to the rim of the domain. It is best differentiated from the stations in Quebec (stations LATQ and MNTQ, Figure 1) and the yellow domain by the sharp contrasts of averaged fast polarizations and the proportion of NULL measurements at each station, respectively. Similar to the green domain, the blue domain has a narrow range of back azimuths in the WNW that yield NULL measurements. Furthermore, permanent stations like PQI and PKME from Levin et al. (2018), which include more events, show a wide cluster of NULL measurements in the northeastern quadrants, corresponding to 0° to 45° azimuth.

Due to the limited number of sites to the north of the Adirondack Mountains, it is difficult to declare the region encompassed by the two stations (LATQ and MNTQ, see their diagrams in the supplement) as a distinct domain. However, we note that the differences of splitting patterns between these stations and the stations within the surrounding domains are clear. In particular, the characteristic reduction of the delay times yielded by the northwestern events, observed at all sites within the green domain, is absent. Delay times at the sites in Quebec do not show systematic reduction for all of the sampled back azimuths. Also characteristic to these sites is the distinctly E-W oriented fast polarization, distinct from the NE-SW fast polarization of the green and blue domains. The noticeably smaller standard deviation of fast polarizations (Figure 9b), particularly in comparison with the stations in the blue domain, suggests that the population of sampled fast orientation systematically shifts to E-W within this region.

### 3.2.2. Domain-wise Fit to an Anisotropic Model by SI Technique

To verify the similarity of splitting behavior within each domain, we tested the domain-wide fit of individual splitting intensities to a common sinusoidal pattern predicted by a particular anisotropic model (Figure 10). Conversely, we also estimated a best-fit sinusoid for the same collection of splitting intensity values using least squares minimization. The similarity

between the predicted and the fitted sinusoids confirms self-consistency of the combined domain-wide datasets, as well as provides a quantitative means for constraining the strength of the anisotropic signal for each domain. The averaged delay time $\delta t$ is constructed on the basis of values returned by the RC method (see Methodology and Data section). Other methods of estimating shear wave splitting (e.g. Minimization of the Transverse component) tend to yield larger delay values for the same data (Wüstefeld & Bokelmann, 2007). The compatibility of the delay values from the RC method and the SI technique is another reason for us to prefer its values in this study.

We see a good agreement in sinusoid functions at three domains. The yellow domain is an exception, as it shows a clear mismatch between the functions constrained by the SI data and predicted by the averaged splitting parameters (Figure 10d). The discrepancy may be explained by a large proportion of measurements defined as NULL. They are not included in the computation of averaged splitting values obtained by the RC technique, but their SI values are included in the estimate of best-fitting sinusoid. The lower amplitude of the curve obtained by fitting SI values indicates that simple averaging that only considers the split measurements may overestimate the delay times in the cases of abundant NULL measurements, as observed in the yellow domain.

### 3.2.3. Geometries and Characterization of the Inferred Domains Boundaries

We drew domain boundaries between groups of stations that show similar splitting behaviors according to our quantitative and qualitative classification schemes described above. We note that the boundaries may change with the addition of more observing sites, and by using different sets of classification criteria. Furthermore, the nature of transitions between domains may also contribute to the complexities for determining the domain geometries. With these caveats, we discuss the boundaries we did draw.

Within our study area, we observe both sharp transitions in splitting behaviors, as well as gradual changes in certain traits that result in provisional boundaries. For instance, the yellow domain shows consistent splitting behavior that is clearly different from the surrounding domains, as supported by the distinct values in all featured quantitative measures. On the other hand, the shift between the red and the green domains appears to occur over greater distances, with some transitional stations such as L59A and TRY in southern New York that contain trait characteristic for both the green and the red domains. Although the boundaries may be better resolved by both increased station density and data number, it is also possible that the nature of the boundaries reflects the underlying anisotropic structure of the upper mantle, which is not necessarily laterally discrete. What should be undisputable from our dataset, however, is the presence of well-defined regions of systematic splitting behavior that are describable with the observations known to vary according to complex anisotropic structures. Despite the variable width of domain boundaries, the distances over which the patterns systematically change between the groups of stations are relatively short compared to the aerial extent encompassed by the stations that share common characteristics. Examination of splitting patterns within each domain may uncover potential details that are otherwise masked by the seemingly coherent regional trends of the averaged splitting parameters.

## 4 Discussion

### 4.1. Comparison with Previous Studies

A number of recent studies (e.g.; Long et al., 2015; Wagner et al., 2012; Yang et al., 2017) have characterized seismic anisotropy beneath the eastern margin of North America using the shear wave splitting method. While there is considerable heterogeneity in specific values of fast polarizations and delays, a number of common aspects emerged from these studies.

Generally, the widespread similarity of averaged fast polarizations, and their overall agreement with the APM direction suggest anisotropy due to the ongoing deformation within the upper mantle due to the motion of the North American plate. This conclusion was also reached by Chen et al. (2018) study that extends into the craton to the northwest of our region. On the other hand, a number of investigators (e.g., Gilligan et al., 2016; White-Gaynor & Nyblade, 2017) focused on the lateral changes in patterns of averaged fast polarizations, seeking to relate them to the local trends of tectonic units, and thus explain them as reflective of anisotropic texture within the continental lithosphere. Also, evidence for multilayered anisotropy has been inferred from back-azimuthal variation of the splitting patterns (Levin, 1999, 2000), as well as anisotropic velocity boundaries detected using directional variations in the nature of mode-converted body waves (Yuan & Levin, 2014).

If we consider the averaged splitting parameters, our results are fully compatible with observations reported by previous studies in the region (Figure 11). The trends of fast polarizations in our study (E-W, and ENE-WSW) and their general uniformity over the study region are consistent with findings of other studies that have characterized the lateral variation of splitting patterns throughout the eastern North America (Long et al., 2015; Yang et al., 2017). In particular, our study region fits into “Region A” defined by Long et al., (2015) which was grouped on the basis of regionally consistent, E-W (average of 77°) trending fast polarization orientations and their smooth lateral variation.

Delay times from our study show patterns of spatial variation similar to those reported by others, although there is a systematic discrepancy in the overall range of delay time values between this study and the previous studies. As discussed in the Results section, this discrepancy likely arises from the choices of measurement methodology. Specifically, the largest delay times are observed in northern Maine, where individual splitting parameters as high as 4 s are also reported by previous studies (Chen et al., 2018; White-gaynor & Nyblade 2017). Similarly, the reported delay times near the southern end of the study area are smaller, with most published studies showing values of about 1 s. Some results even report values over 2 s. While our delay time values show a similar trend, the range of values reported by our study is significantly smaller, with a maximum delay time under 1.4 s in northern Maine.

With good back azimuthal coverage emphasized by our study, we document clear evidence for directional variation of the splitting parameters at all of our stations. Given its obviously systematic nature (e.g. directional patterns in the Adirondacks, section 3.2.1.3) this variation presents an obvious challenge to the interpretation of single pairs of splitting parameters assigned to stations on the basis of averaging the observed values, or else by fitting Splitting Intensity patterns. Nevertheless, we argue that single-station values are useful, for the following reasons: a) they provide a means of comparing our findings to those of other studies that chose to average the values; b) they serve as a proxy for Earth’s properties and, having been systematically derived, offer insight into lateral variation in them; and c) we use single-station values and associated measures of splitting parameters’ variability (Figure 9) as means of delineating regional domains that are the focus of this study.

At the same time, we stress that directional patterns found at most of our sites (Figure 8; figures S1 to S33) suggest vertically varying anisotropic properties previously proposed for this part of eastern North America (cf. Levin et al., 1999, 2000). Our finding of at least four distinct anisotropic domains in Northern Appalachians contradicts the earlier publications by Levin et al. (2000ab) that argued for a uniform regional layering of anisotropic properties. The key difference between those studies and the present one is in the quantity of data, both in terms of the length of observation, and especially in terms of the lateral sampling of the region.

Complex anisotropy is known to cause discrepancies between the apparent splitting parameters quantified using different technique (e.g. Long & van der Hilst, 2005; Wüstefeld & Bokelmann, 2007). Even though the directional variation of individual delay times is expected, our highest delay times obtained using the RC and the SI methods do not exceed 2.5 seconds, smaller than the maximum of 4 seconds obtained by SC method used in other studies. Although different measured values complicate the comparison between the results of this study and the previous studies, all data sets nonetheless seem to report a similar geographical pattern of splitting parameters, including the general coherency of averaged fast polarizations and lateral variation of delay times. In addition, the agreement between our two sets of splitting parameters, yielded by SI technique and RC technique, provides assurance for the reliability of our data.

### 4.2. Comparison with Other Geological and Geophysical Observables

The tectonic terranes presently exposed in the Northern Appalachians can be linked to episodes of crustal deformation from multiple collisional events that comprise the Appalachian Orogeny (Hatcher, 2010). Geological evidence defines three main orogenic events; the accretion of a volcanic arc during the Ordovician Taconic orogeny, accretion of microcontinents during the Devonian Acadian orogeny (Hibbard et al., 2006), and finally the culminating continental collision during the Permian Alleghenian orogeny. Boundaries between individual terranes making up the Appalachian Orogen are delineated by differences in lithologies and detrital zircon signatures that are interpreted as evidence for subduction-related magmatism and different sediment provenances pertaining to the origin of specific terranes (e.g., Hibbard & Waldron, 2009; Karabinos et al., 1998). The increased details of geological and geochemical observations at the surface are reconciled by invoking contributions from deep structures, such as changing subduction polarities and slab detachments, providing implications for what structures should exist at depth (e.g., Karabinos et al., 2017). The likely heterogeneity of anisotropic properties from the deformation within the upper mantle should be reflected in lateral variations of shear wave splitting parameters. However, as illustrated by single-event splitting maps in Figure 3, the observed lateral variation reflects both the scale of the anisotropic structures at depth and the direction of illumination by shear waves. Consequently, it is important to include directional patterns in splitting values (e.g.; Figure 8) in the definitions of anisotropic domains that may correspond to tectonic terranes or features of the upper mantle shaped by past tectonic episodes.

The attempts to discern subsurface volumes with anisotropic properties, and by extension the relative contributions from the lithosphere and the asthenosphere in the apparent observations, have in part relied on comparisons with other geological and geophysical observables. For example, an alignment of tectonic boundaries and the orientations of fast polarization of split shear waves may be taken to signify a substantial lithospheric contribution to the apparent splitting. Furthermore, sharp lateral variation observed between

two closely spaced stations can suggest changes in anisotropy that are relatively close to the surface (e.g., Aragon et al., 2017). Here we compare our station-averaged splitting parameters and the spatial distribution of our station groups with surface geology (Figure 12a) and with the shear wave velocity distribution at a depth of 90 km in the model of Shen and Ritzwoller (2016) (Figure 12b). Since seismic velocity discontinuities detected by scattered body waves place the lithosphere-asthenosphere boundary in Northern Appalachians at 85-100 km depth (e.g. Abt et al., 2010; Rychert et al., 2007), the variations in velocity seen at this depth should be representative of the overlying lithospheric structure.

At the first glance, the obvious mismatch between the averaged orientations of fast polarizations and the trends of tectonic features is striking. With the possible exception of a small area in southern Quebec and northwestern Maine, fast polarizations remain oblique to the trends of individual terrane boundaries, including that of the Appalachian Front, and do not imitate their changes from south to north (Figure 1 and Figure 12a). However, this mismatch needs to be considered in the context of directional variability in splitting parameters seen at most sites of the region. As explored in earlier papers by Levin et al., (1999; 2000) and also by Yuan and Levin (2014), the true orientation of the anisotropic fabric at various depth levels is guaranteed to be different from the average. It is therefore possible that the lithospheric mantle of the region does contain anisotropic textures aligned with terrane boundaries, though a formal modeling effort is needed to ascertain this. On the other hand, the geometry of domain boundaries shows some correlations with both the surface geology and the upper mantle structure. In particular, the Adirondack mountains in northern New York correspond spatially to the green domain. The characteristic directional patterns of fast polarizations (see section 3.2.1.3) suggest a localized volume within the underlying upper mantle that possesses a distinct arrangement of vertically varying anisotropy.

The distinct character of the Proterozoic Adirondack mountains is not surprising, as this is the only area in our study that belongs to Laurentia (Whitmeyer & Karlstrom, 2007), and has not been affected by the orogenic processes during the assembly of Pangea. Consequently, the lithosphere of this area and the anisotropy-forming fabric within it dates to ~1 Ga age of the Grenville Orogeny (Hynes & Rivers, 2010), and may even pre-date it. To explain the timing of emplacement of anorthosite bodies in the Adirondacks, Mclelland et al. (2010) proposed an episode of lithospheric foundering and replacement, a process likely recorded in the residual lithospheric fabric. Additionally, the lithosphere of this domain may be experiencing a modern-day alteration, as suggested by the surface wave imaging by Yang and Gao (2018).

In the domains within the Appalachian Orogen (red, yellow, blue) there is no apparent correlation between averaged splitting parameters and individual terranes (e.g. Avalonia, Gander) that represent different tectonic units assembled in the Paleozoic. Instead, similar patterns of splitting enclose areas with multiple terranes identified by surface geology. This likely points to the lithospheric mantle, or deeper origin of the differences in their splitting patterns. This is especially clear in Maine where individual tectonic units of the Appalachians are significantly wider relative to their extensions further south (cf. Figure 1, Figure 12a), but show high similarity in anisotropic signature. The vertical extent of the lithosphere is similar in these domains (Abt et al., 2010), however they belong to two parts of the Appalachian Orogen that may have experiences different tectonic histories (e.g. Hatcher, 2010). Distinct lithosphere structure may be the cause for the clear difference in strength of the spitting signal, ~0.5 s in New Jersey vs over 1 s in Maine. However, the local variation in sub-lithospheric flow may also play a role, especially considering the previously documented

association of the yellow domain with a deep-seated (100 – 300 km) North Appalachian Anomaly (NAA) (Schmandt & Lin, 2014; Menke et al., 2016; Levin et al., 2018).

The boundaries of the yellow domain appear to be aligned with the slow feature at greater depths seen in most tomographic studies with sensitivity to the 50 – 150 km range (Shen & Ritzwoller, 2016; Yang & Gao, 2018; Figure 12b). The feature is located beneath Vermont and New Hampshire, and spatially coincides with the deeper NAA anomaly. The near-absence of splitting in this domain is puzzling. It implies the lithosphere lacking a well-developed texture, a significant localized difference from surrounding areas that share its Paleozoic tectonic history. A possible cause of this local anomaly in both seismic velocity (slow) and anisotropy (absent) may be the influence of the deeper asthenospheric upwelling proposed by Menke et al., 2016 and Levin et al., 2018. It is interesting to consider the possibility that lithosphere alteration by the passage of a hot spot (Eaton & Frederiksen, 2007; Sleep, 1990) left an imprint that presently guides the upwelling to this region.

Other parts of the region also show a degree of correlation between the anisotropic signature and seismic velocity at lithospheric depths. Specifically, the green domain over the Adirondacks seems to better match the regions of intermediate velocities adjacent to the slow anomaly. The stations of red domain and the two sites within the Grenville province, match with the regions where the velocities are relatively high. The better correspondence between the domain geometries and the velocity structure at the depth of 90 km suggests that the different domains may reflect the differences in the seismic properties within the lithospheric mantle or near the lithosphere-asthenosphere boundary of the region. Consequently, the apparent variation of the seismic velocities determined under the assumption of isotropy may be controlled in part by the variation of anisotropic properties.

### 4.3. Vertically Incoherent Deformation

The observations of shear wave splitting from the adjacent segments of the Appalachian Mountains, including Newfoundland, Canada by Gilligan et al. (2016) and southeastern United States by White-Gaynor & Nyblade (2018) and Long et al. (2015) report strong correlation between the orientations of averaged fast polarization and the surficial tectonic and topographic features. The similarity between the fast polarization and the tectonic features is cited as evidence for strong relative contributions from the fossil lithospheric fabrics, as well as for coherent deformation of the crust and the lithospheric mantle (Silver, 1996). For the region investigated by this study, however, we do not observe this clear correlation with either the regional topography or the well-defined terrane boundaries (Figures 1, 12A).

As discussed in the previous section, the lithospheric contribution to the apparent splitting we have measured is undisputable. However, as we do not see the match between the average splitting directions and the features of surface geology, we conclude that the mantle lithosphere must have a fabric distinct from that of the shallow crust. This in turn implies vertical decoupling of the deformation between the lithosphere and the crust during the Appalachian Orogeny which was the last tectonic event to affect the entire region. Additionally, the strong correlation of average fast polarizations to the APM throughout the region suggests that a dominant contribution to the splitting pattern is from plate motion relative to the asthenosphere, a finding similar to that of Long et al. (2015).

### 4.4. Non-uniform Upper Mantle Anisotropy, and the Motivation for Forward Modeling

The weaker lithospheric contributions are difficult to quantify and characterize by simply using the station-averaged splitting parameters because the signatures indicative of finer-scale lateral differences may be disregarded by the averaging procedures. Local variations of splitting patterns detected through our procedure allow consideration of all individual splitting parameters and characterization of heterogeneous splitting behaviors at a finer scale than the previous studies. With improved back azimuthal coverage, we show that directional variation of the splitting parameters is not uniform throughout eastern North America. Rather, the region can be divided into discrete domains that show distinct patterns of directional variation. All stations within each domain share similar splitting behavior, likely modulated by a common arrangement of vertically varying anisotropy. The transitions between domains occur over distances much shorter than the areas encompassed by the domains. The sharp boundaries, depending on the scale of the observed lateral variation, may be attributed to processes and structures proposed at various scales and depths, including remnant tectonic features, local geodynamic processes, or the topography of the lithosphere-asthenosphere boundary.

Poor depth resolution of the shear wave splitting methods poses difficulties for attributing the anisotropic structures to specific regions of the upper mantle and lies at the root of the ongoing debate about the relative contributions to the signal from modern and fossil rock fabrics.
Studies that utilize station-averaged values of splitting as constraints for geodynamic calculations often find the need to consider both contributions, especially in North America following the deployment of the USArray (e.g. Wang & Becker, 2019; Zhou et al., 2018). However, station averages that reduce the complexity of shear-wave splitting signal to two numbers are an imperfect proxy. The model constrainable by the station-averaged splitting parameters therefore may be only sufficient for deeper, more pervasive sources of anisotropy such as the relative lithosphere-asthenosphere plate motion. It is guaranteed to leave a large fraction of the signal unexplained.

Two alternatives to using station averages present themselves, both involving explicit forward modeling of directional shear wave splitting variations. One choice is to conduct forward modeling of the observed directional data (e.g., Yuan & Levin, 2014), characterize the vertical variation of anisotropic properties at different locations and use the results as constraints for the next generation of geodynamic computations. Another is to build the anticipation of directional variability in XKS splitting into the forward-modeling components of algorithms like those used in Wang and Becker (2019).

Either way, the evidence for regional variation of the splitting behavior documented by directional patterns in individual splitting parameters as done in this study strongly supports the need to vary the anisotropic models locally. Sharp lateral variation we have documented offers the means to constrain shallower features. Furthermore, specific combinations of individual splitting parameters in the dataset from anisotropic domains (e.g. Figure 10) provides more quantitative features that may be used to gauge the degree of fit in geodynamic predictions of mantle deformation.

## 5. Summary and Implications

1. For 33 long-running stations in eastern North America, we collected new sets of averaged and individual splitting parameters of core-refracted shear phases using a uniform set of 61 seismic events chosen to optimize back azimuthal coverage. We produced ~1400 new measurements of shear wave splitting. Combining these observations with our recent results for another subset of sites in the same region, we present an integrated data set of ~2000 observations for 41 locations with 3 or more years of data collection.

2. We document a strategy for creating a systematic consistent characterization of anisotropic properties in a region composed of numerous distinct tectonic units. A key element of the strategy is the significance of directional variation in shear wave splitting. We develop qualitative and quantitative measures of this variation and use them as additional attributes that provide constraints on the subsurface structure of the region.
   We employ a combination of single-phase measurements (the rotation-correlation method) and the multi-event estimates of anisotropy attributes (the splitting intensity method) and show that their results are internally compatible in terms of inferred orientations of the fast polarization, and the size of delays between fast and slow components of split shear waves.

3. Station-averaged splitting parameters show geographical patterns compatible with those described in the previous studies. In particular, we confirm a broad alignment between the average fast polarization and the absolute plate motion (APM) in a hot-spot reference frame. Significantly, most station-averaged fast polarizations we constrain differ from the APM by ~10° in the clockwise direction.

4. With few exceptions, we do not find any evidence for averaged fast polarization being aligned with tectonic features or the topographic fabric of the region. This is in contrast to results of some recent publications and may be a reflection of longer observing periods and an emphasis on directional sampling in our study.

5. The overall strength of seismic anisotropy, as quantified by the averaged station delays, has a clear geographic pattern, with smaller (~0.5 s) delays found to the south of 44° and larger (up to 1.4 s) seen farther to the north. The transition between smaller and larger delay values manifests itself differently depending on the method used to estimate it. Delay values obtained via a multi-event fitting procedure based on splitting intensity values suggest relatively uniform regions with distinct delays of different size, and an abrupt transition between them. Results of averaging single-phase delay measurements have larger error bars and are compatible with a gradual regional trend.

6. At all sites, we find directional variation of individual splitting parameters consistent with vertically varying anisotropic properties. Additionally, we identify four geographic domains that are defined by similar modes of directional variation. We develop a set of criteria that are used to group sites into domains. These include the average size of delays and the average direction of fast polarization; the degree of variance in both parameters; the fraction of NULL (absence of splitting and/or inability to measure) observations; and the patterns of variation with respect to back

azimuth and incidence angle. Our results build upon the long-standing recognition of vertical stratification in the anisotropic properties of eastern North America, documenting a regionalized nature of this stratification.

7. Regionally consistent anisotropic properties within individual domains change over relatively short distances, suggesting a significant role for the rock fabric preserved within the mantle lithosphere of the North American continent. The ability to map the lithospheric domains offers a unique way to identify the building blocks of the continent.

8. In particular, the distinct nature of the anisotropic structure associated with Grenville-age Adirondack Mountains suggests an association with the lithosphere of Laurentia. An extension of this domain into the Paleozoic Appalachian Orogen suggests continuity of the mantle lithosphere underlying the tectonic boundary (the Appalachian Front) that separates them. Conversely, the clear difference between the Adirondack Mountains domain and the domain including the southernmost New York and New Jersey implies differences in the origin and/or history of the entire lithosphere, from the crust to the bottom of the plate.

9. Our study confirms the existence and further enhances the definition of an area where shear wave splitting does not occur, or else is very weak. The domain with weak/absent splitting spatially coincides with the North Appalachian Anomaly, an area of low shear wave velocity in the upper mantle. The absence of lithospheric anisotropy signature (splitting) from any direction of wave propagation is a strong departure from the broader regional trend. Given tectonic similarity of the no-splitting domain and areas to its north and south, the plausible explanation is an erasure of the fabric by events post-dating the assembly of the Appalachian Orogen.

10. In conclusion, our study presents a template for constructive utilization of complexity in the shear wave splitting data. We emphasize that this complexity is a signal that further bolsters our ability to probe the interior structure of tectonically complex regions.

**Acknowledgments and Data**

This project was supported by the NSF Earthscope grant EAR-1735912, as well as the support from Rutgers School of Graduate Studies for the first author. The Aresty Undergraduate Research Assistantship for Stephen Elkington and Janine Hlavaty was instrumental for their participation in this work.

The figures were constructed using Generic Mapping Tool (Wessel et al., 2013) and MATLAB software. The shear wave splitting parameters were measured using a version of SplitLab software (Wüstefeld et al., 2008) integrated with the modules for calculating Splitting Intensity values developed in Deng et al. (2017). The data for the project were obtained from and can be accessed at the IRIS Data Management Center (https://ds.iris.edu/ds/nodes/dmc/). The specific seismic networks that provided data for this study include: Central and Eastern US Network (https://doi.org/10.7914/SN/N4), Lamont-Doherty Cooperative Seismographic Network (http://www.ldeo.columbia.edu/LCSN/), New England Seismic Network (https://doi.org/10.7914/SN/NE), Portable Observatories for Lithospheric Analysis and Research Investigating Seismicity (POLARIS)

(http://www.polarisnet.ca/network/polaris-network-locations.html), United States National Seismic Network (https://doi.org/10.7914/SN/US), and Canadian National Seismograph Network (https://doi.org/10.7914/SN/CN).

We gratefully acknowledge the three anonymous reviewers for their helpful comments and suggestions that significantly improved this manuscript.

## References

Abt, D. L., Fischer, K. M., French, S. W., Ford, H. A., Yuan, H., & Romanowicz, B. (2010). North American lithospheric discontinuity structure imaged by Ps and Sp receiver functions. *Journal of Geophysical Research*, *115*, 1–24. https://doi.org/10.1029/2009JB006914

Aragon, J., Long, M. D., & Benoit, M. H. (2017). Lateral Variations in SKS Splitting Across the MAGIC Array, Central Appalachians. *Geochemistry, Geophysics, Geosystems*, *18*, 4136–4155. https://doi.org/10.1002/2017GC007169

Barruol, G., Silver, P. G., & Vauchez, A. (1997). Seismic anisotropy in the eastern United States : Deep structure of a complex continental plate. *Journal of Geophysical Research*, *102*(B4), 8329–8348.

Bowman, J. R., & Ando, M. (1987). Shear-wave splitting in the upper-mantle wedge above the Tonga subduction zone. *Geophysical Journal of the Royal Astronomical Society*, *88*(1), 25–41. https://doi.org/10.1111/j.1365-246X.1987.tb01367.x

Chen, X., Li, Y., & Levin, V. (2018). Shear Wave Splitting Beneath Eastern North American Continent: Evidence for a Multi-layered and Laterally Variable Anisotropic Structure. *Geochemistry, Geophysics, Geosystems*, *19*, 1–15. https://doi.org/10.1029/2018GC007646

Chevrot, S. (2000). Multichannel analysis of shear wave splitting. *Journal of Geophysical Research: Solid Earth*, *105*(B9), 21579–21590. https://doi.org/10.1029/2000JB900199

Crampin, S. (1977). A review of the effects of anisotropic layering on the propagation of seismic waves. *Geophysical Journal of the Royal Astronomical Society*, *49*(1), 9–27.

Deng, J., Long, M. D., Creasy, N., Wagner, L., Beck, S., Zandt, G., … Minaya, E. (2017). Lowermost mantle anisotropy near the eastern edge of the Pacific LLSVP: Constraints from SKS-SKKS splitting intensity measurements. *Geophysical Journal International*, *210*(2), 774–786. https://doi.org/10.1093/gji/ggx190

Eaton, D. W., & Frederiksen, A. (2007). Seismic evidence for convection-driven motion of the North American plate. *Nature*, *446*(March), 428–431. https://doi.org/10.1038/nature05675

Garrity, B. C. P., & Soller, D. R. (2005). Database of the Geologic Map of North America — Adapted from the Map by J . C . Reed , Jr . and others ( 2005 ). *U.S. Geological Survery Data Series*, *424*.

Gilligan, A., Bastow, I. D., Watson, E., Darbyshire, F. A., Levin, V., Menke, W., … Petrescu,

L. (2016). Lithospheric deformation in the Canadian Appalachians : evidence from shear wave splitting. *Geophysical Journal International*, *206*, 1273–1280. https://doi.org/10.1093/gji/ggw207

Gripp, A. E., & Gordon, R. G. (2002). Young tracks of hotspots and current plate velocities. *Geophysical Journal International*, *150*, 321–361.

Hatcher, R. D. (2010). The Appalachian orogen: A brief summary. *The Geological Society of America Memoir*, *206*(01), 01-19. https://doi.org/10.1130/2010.1206(01).

Hibbard, J., van Staal, C. R., Rankin D. W., Williams, H., (2006) Lithotectnic map of the Appalachian Orogen, Canada-United States of America [map]. (ca 1:1500000) New Brunswick, Newfoundland : Natural Resources Canada.

Hibbard, J., & Waldron, J. W. F. (2009). Truncation and translation of Appalachian promontories: Mid-Paleozoic strike-slip tectonics and basin initiation. *Geology*, *37*(6), 487–490. https://doi.org/10.1130/G25614A.1

Hynes, A., & Rivers, T. (2010). Protracted continental collision — evidence from the Grenville Orogen 1, *620*, 591–620. https://doi.org/10.1139/E10-003

Karabinos, P. M., Macdonald, F. A., & Crowley, J. L. (2017). Bridging the Gap Between the Foreland and Hinterland I : Geochronology and Plate Tectonic Geometry of Ordovician Magmatism and Terrane Accretion on the Laurentian Margin of New England. *American Journal of Science*, *317*, 515–554. https://doi.org/10.2475/05.2017.01

Karabinos, P., Samson, S. D., Hepburn, J. C., & Stoll, H. M. (1998). Taconian orogeny in the New England Appalachians: Collision between Laurentia and the Shelburne Falls arc. *Geology*, *26*(3), 215–218. https://doi.org/10.1130/0091-7613(1998)026<0215:TOITNE>2.3.CO;2

Levin, V., Long, M. D., Skryzalin, P., Li, Y., & López, I. (2018). Seismic evidence for a recently formed mantle upwelling beneath New England. *Geology*, *46*(1), 87–90. https://doi.org/10.1130/G39641.1

Levin, V., Menke, W., & Park, J. (1999). Shear wave splitting in the Appalachians and the Urals: A case for multilayered anisotropy. *Journal of Geophysical Research*, *104*(B8), 17975–17993.

Levin, V., Menke, W., & Park, J. (2000). No regional anisotropic domains in the northeastern US Appalachians. *Journal of Geophysical Research: Solid Earth*, *105*(B8), 19029–19042. https://doi.org/10.1029/2000JB900123

Levin, V., Park, J., Brandon, M. T., & Menke, W. (2000). Thinning of the upper mantle during late Paleozoic Appalachian orogenesis, (3), 239–242.

Li, Y., Levin, V., Chen, X. (2017) Seismic Anisotropy Beneath Eastern North America : Results from Multi-Event Inversion, AGU Fall Meeting, Abstract T11A-0436.

Long, M. D., & Becker, T. W. (2010). Mantle dynamics and seismic anisotropy. *Earth and Planetary Science Letters*, *297*(3–4), 341–354. https://doi.org/10.1016/j.epsl.2010.06.036

Long, M. D., Jackson, K. G., & McNamara, J. F. (2015). SKS splitting beneath Transportable Array stations in eastern North America and the signature of past lithospheric deformation. *Geochemistry, Geophysics, Geosystems*, *17*, 2–15. https://doi.org/10.1002/2014GC005684.Key

Long, M. D., & Silver, P. G. (2009). Shear wave splitting and mantle anisotropy: Measurements, interpretations, and new directions. *Surveys in Geophysics*, *30*, 407–461. https://doi.org/10.1007/s10712-009-9075-1

Long, M. D., & van der Hilst, R. D. (2005). Estimating shear-wave splitting parameters from broadband recordings in Japan: A comparison of three methods. *Bulletin of the Seismological Society of America*, *95*(4), 1346–1358. https://doi.org/10.1785/0120040107

Mclelland, J. M., Selleck, B. W., Hamilton, M. A., & Bickford, M. E. (2010). LATE- TO POST-TECTONIC SETTING OF SOME MAJOR PROTEROZOIC ANORTHOSITE – MANGERITE – CHARNOCKITE – GRANITE ( AMCG ) SUITES, *48*, 729–750.

Nicolas, A. & Christensen, N. I., (1987). Formation of Anisotropy in Upper Mantle Peridotites - A Review. In K. Fuchs & C. Froidevaux (Eds.), Composition, Strucutre, and Dynamics of the Lithosphere-Asthenosphere System. (Vol. 16, pp. 111-123). Washington, DC: American Geophysical Union.

Park, J., & Levin, V. (2002). Seismic Anisotropy: Tracing Plate Dynamics in the Mantle. *Science*, *296*(5567), 485–489. https://doi.org/10.1126/science.1067319

Rychert, C. A., Rondenay, S., & Fischer, K. M. (2007). P -to- S and S -to- P imaging of a sharp lithosphere-asthenosphere boundary beneath eastern North America. *Journal of Geophysical Research*, *112*, 1–21. https://doi.org/10.1029/2006JB004619

Savage, M. K. (1999). Seismic Anisotropy and Mantle Deformation: What Have We Learned From Shear Wave Splitting? *Reviews of Geophysics*, *37*(1), 65–106.

Schmandt, B., & Lin, F. (2014). P and S wave tomography of the mantle beneath the United States. *Geophysical Research Letters*, *41*, 6342–6349. https://doi.org/10.1002/2014GL061231.Received

Shen, W., & Ritzwoller, M. H. (2016). Crustal and uppermost mantle structure beneath the United States. *Journal of Geophysical Research: Solid Earth*, *121*, 4306–4342. https://doi.org/10.1002/2016JB012887.Received

Silver, P. G. (1996). SEISMIC ANISOTROPY BENEATH THE CONTINENTS: Probing the Depths of Geology. *Annual Review of Earth and Planetary Sciences*, *24*(1), 385–432. https://doi.org/10.1146/annurev.earth.24.1.385

Silver, P. G., & Chan, W. W. (1988). Implications for continental structure and evolution from seismic anisotropy. *Nature*, *335*(1), 34–39.

Silver, P. G., & Chan, W. W. (1991). Shear Wave Splitting and Subcontinental Mantle Deformation. *Journal of Geophysical Research*, *96*(B10), 16429–16454.

Silver, P. G., & Savage, M. K. (1994). The interpretation of shear-wave splitting parameters

in the presence of two anisotropic layers. *Geophysical Journal International*, *119*, 949–963.

Sleep, N. H. (1990). Monteregian Hotspot Track : A Long-Lived Mantle Plume. *Journal of Geophysical Research*, *95*(B13), 21983–21990.

Thomas, W. A. (2006). Tectonic inheritance at a continental margin. *GSA Today*, *16*(2), 4–11. https://doi.org/10.1130/1052-5173(2006)016<4

Vinnik, L. P., Farra, V., & Romanowicz, B. (1989). Azimuthal Anisotropy in the Earth From Observations of SKS At Geoscope and Nars Broadband Stations. *Bulletin of the Seismological Society of America*, *79*(5), 1542–1558.

Wagner, L. S., Long, M. D., Johnston, M. D., & Benoit, M. H. (2012). Lithospheric and asthenospheric contributions to shear-wave splitting observations in the southeastern United States. *Earth and Planetary Science Letters*, *341–344*, 128–138. https://doi.org/10.1016/j.epsl.2012.06.020

Wang, W., & Becker, T. W. (2019). Upper mantle seismic anisotropy as a constraint for mantle flow and continental dynamics of the North American plate. *Earth and Planetary Science Letters*, *514*, 143–155. https://doi.org/10.1016/j.epsl.2019.03.019

White-gaynor, A. L., & Nyblade, A. A. (2017). Shear wave splitting across the Mid-Atlantic region of North America : A fossil anisotropy interpretation. *Geology*, *45*(6), 555–558. https://doi.org/10.1130/G38794.1

Whitmeyer, S. J., & Karlstrom, K. E. (2007). Tectonic model for the Proterozoic growth of North America. *Geosphere*, *3*(4), 220–259. https://doi.org/10.1130/GES00055.1

Wüstefeld, A., & Bokelmann, G. (2007). Null Detection in Shear-Wave Splitting Measurements. *Bulletin of the Seismological Society of America*, *97*(4), 1204–1211. https://doi.org/10.1785/0120060190

Wüstefeld, A., Bokelmann, G., Zaroli, C., & Barruol, G. (2008). SplitLab: A shear-wave splitting environment in Matlab. *Computers & Geosciences*, *34*, 515–528. https://doi.org/10.1016/j.cageo.2007.08.002

Yang, B. B., Liu, Y., Dahm, H., Liu, K. H., & Gao, S. S. (2017). Seismic azimuthal anisotropy beneath the eastern United States and its geodynamic implications. *Geophysical Research Letters*, *44*, 2670–2678. https://doi.org/10.1002/2016GL071227

Yang, X., & Gao, H. (2018). Full-Wave Seismic Tomography in the Northeastern United States : New Insights Into the Uplift Mechanism of the Adirondack Mountains. *Geophysical Research Letters*, *45*, 5992–6000. https://doi.org/10.1029/2018GL078438

Yuan, H., & Levin, V. (2014). Stratified seismic anisotropy and the lithosphere-asthenosphere boundary beneath eastern North America. *Journal of Geophysical Research: Solid Earth*, *119*, 3096–3114. https://doi.org/10.1002/2013JB010785.Received

Zhang, S., & Karato, S. (1995). Lattice preferred orientation of olivine aggregates deformed in simple shear. *Nature*. https://doi.org/10.1038/375774a0

Zhou, Q., Hu, J., Liu, L., Chaparro, T., & Stegman, D. R. (2018). Western U . S . seismic anisotropy revealing complex mantle dynamics. *Earth and Planetary Science Letters*, *500*, 156–167. https://doi.org/10.1016/j.epsl.2018.08.015

Geological Survey of Canada (1989): Canadian National Seismograph Network. International Federation of Digital Seismograph Networks. Other/Seismic Network. 10.7914/SN/CN

Albuquerque Seismological Laboratory (ASL)/USGS (1994): New England Seismic Network. International Federation of Digital Seismograph Networks. Other/Seismic Network. 10.7914/SN/NE

Albuquerque Seismological Laboratory (ASL)/USGS (1990): United States National Seismic Network. International Federation of Digital Seismograph Networks. Other/Seismic Network. 10.7914/SN/US

UC San Diego (2013): Central and Eastern US Network. International Federation of Digital Seismograph Networks. Other/Seismic Network. 10.7914/SN/N4

IRIS Transportable Array (2003): USArray Transportable Array. International Federation of Digital Seismograph Networks. Other/Seismic Network. 10.7914/SN/TA

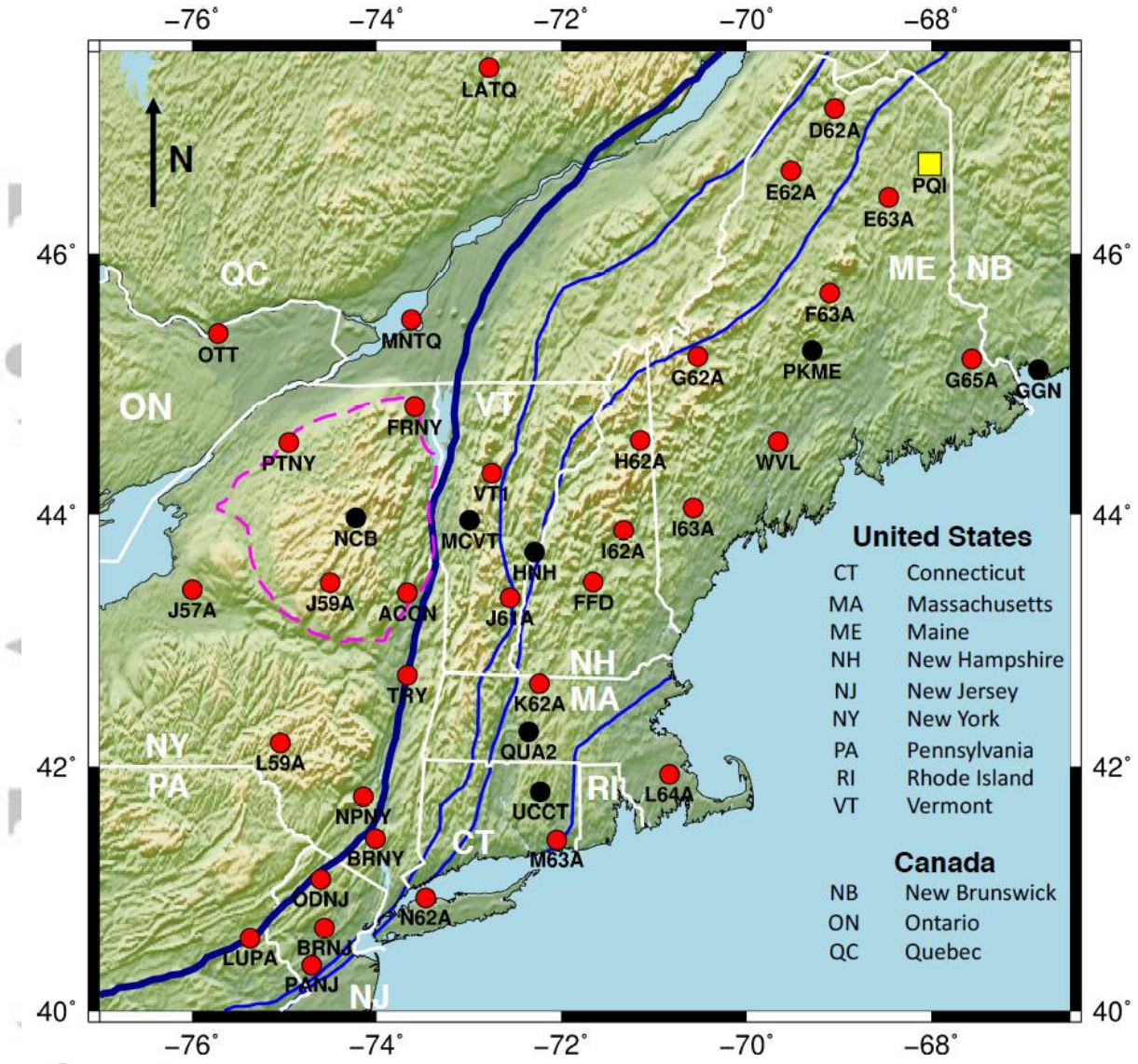


**Figure 1.** The distribution of featured stations in eastern North America. The red circles indicate long-running stations that yielded new datasets for this study. The black circles indicate the stations included from Levin et al. (2018) and Li et al. (2017) to improve the station density. Station PQI, marked in yellow, was used to create the template event list for homogenizing the datasets. The blue lines demark the major geological boundaries pertaining to the tectonic history of the region, modified from the United States Geological Survey basement domain map (http://mrdata.usgs .gov./ds-898). The thick blue line indicates the Appalachian Front, while the thin blue lines are terrane boundaries separating the Taconic Belt, Gander, and Avalonia, respectively from west to east. The magenta dashed line outlines the aerial extent of Adirondack mountains.

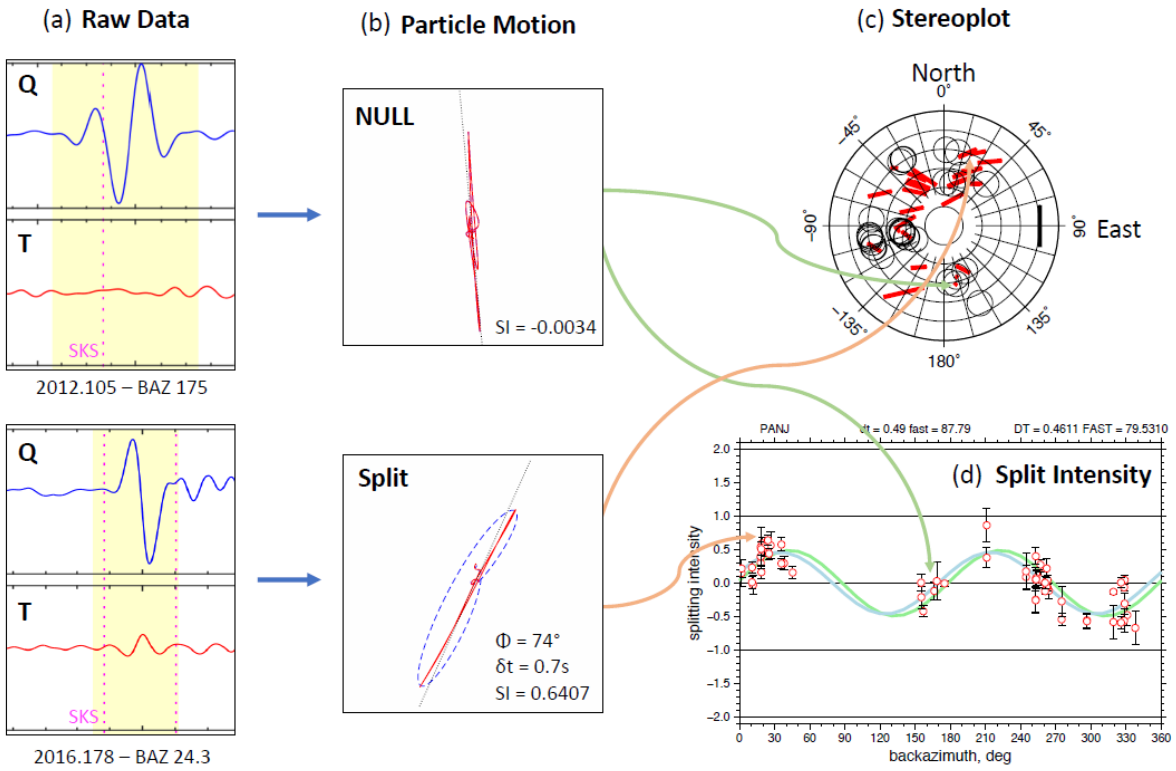


**Figure 2.** The workflow to obtain the datasets used to characterize laterally varying splitting behaviors. The example is from the station PANJ. a) shows examples of SKS signals rotated to LQT (ray-based) coordinate system. The blue line shows the radial component, and the red line shows the transverse component. b) shows the particle motions of waves. The top panel illustrates a wave that is not split (NULL), forming a rectilinear particle motion. The bottom panel shows a split wave, forming an elliptical particle motion. c) an example of a polar coordinates (back azimuth and incidence angle) diagram referred to as the stereonet, displaying all individual splitting parameters measured at a station. Concentric circles show values of inclination angles, from 0 at the center to 18° at the rim, with 3° increments. Thus, data closer to the center of the stereonet corresponds to more vertical rays. The black circles indicate NULL measurements and the red bars indicate split measurements. Bars are scaled proportional to the delay times and aligned with the orientations of fast polarizations, North being up. The black bar near 90° represents 1 s delay time for scale. d) shows the sinusoidal curves calculated from the individual splitting intensities. The blue line is the sinusoid that best-fit the splitting intensity values, and the green line is the sinusoid predicted from the averaged splitting parameters.

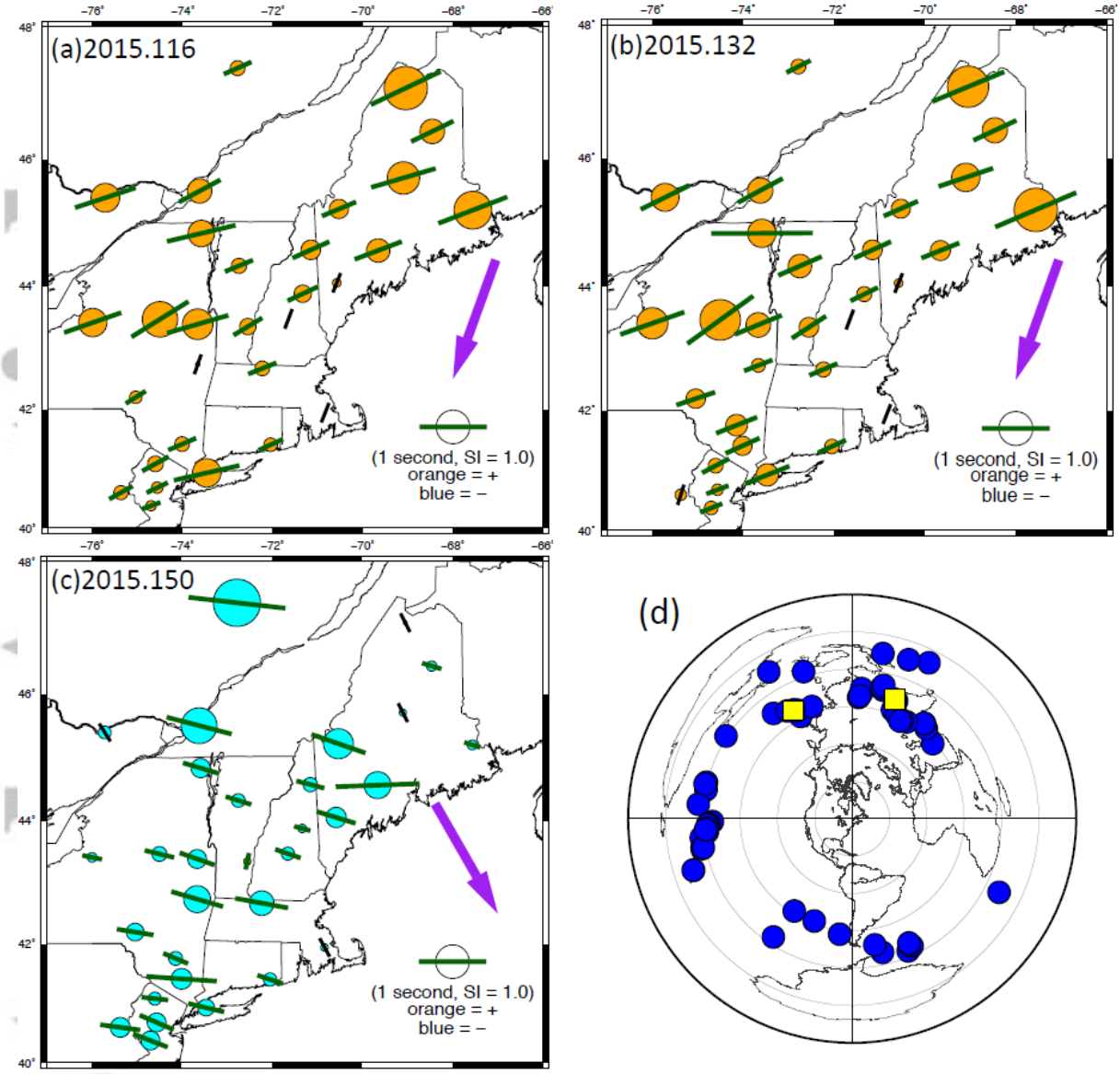


**Figure 3**. Example of individual splitting parameters and splitting intensity (SI) yielded by three events that occurred in 2015, labeled with respective Julian days. The green bars align with the estimated fast polarization orientations and are scaled in proportion to the delay times. The purple arrows indicate the direction of wave propagation. The circles are scaled proportional to the magnitude of SI values; the orange circles indicate positive values and the blue circles indicate negative values. Events 2015.116 (a) and 2015.132 (b) share similar direction of wave propagation from NNE and yield very similar splitting pattern. Event 2015.150 (c) propagates from NNW, and the splitting pattern is starkly different. (d) shows the distribution of 61 selected events displayed in azimuthal equidistant projection centered at our study area. The grey circles indicate the aerial extent encompassed by discrete epicentral distances, starting with 0° at the center and increasing with increments of 30° towards the rim. The yellow squares indicate the source locations corresponding to the events features in panels (a), (b), and (c).

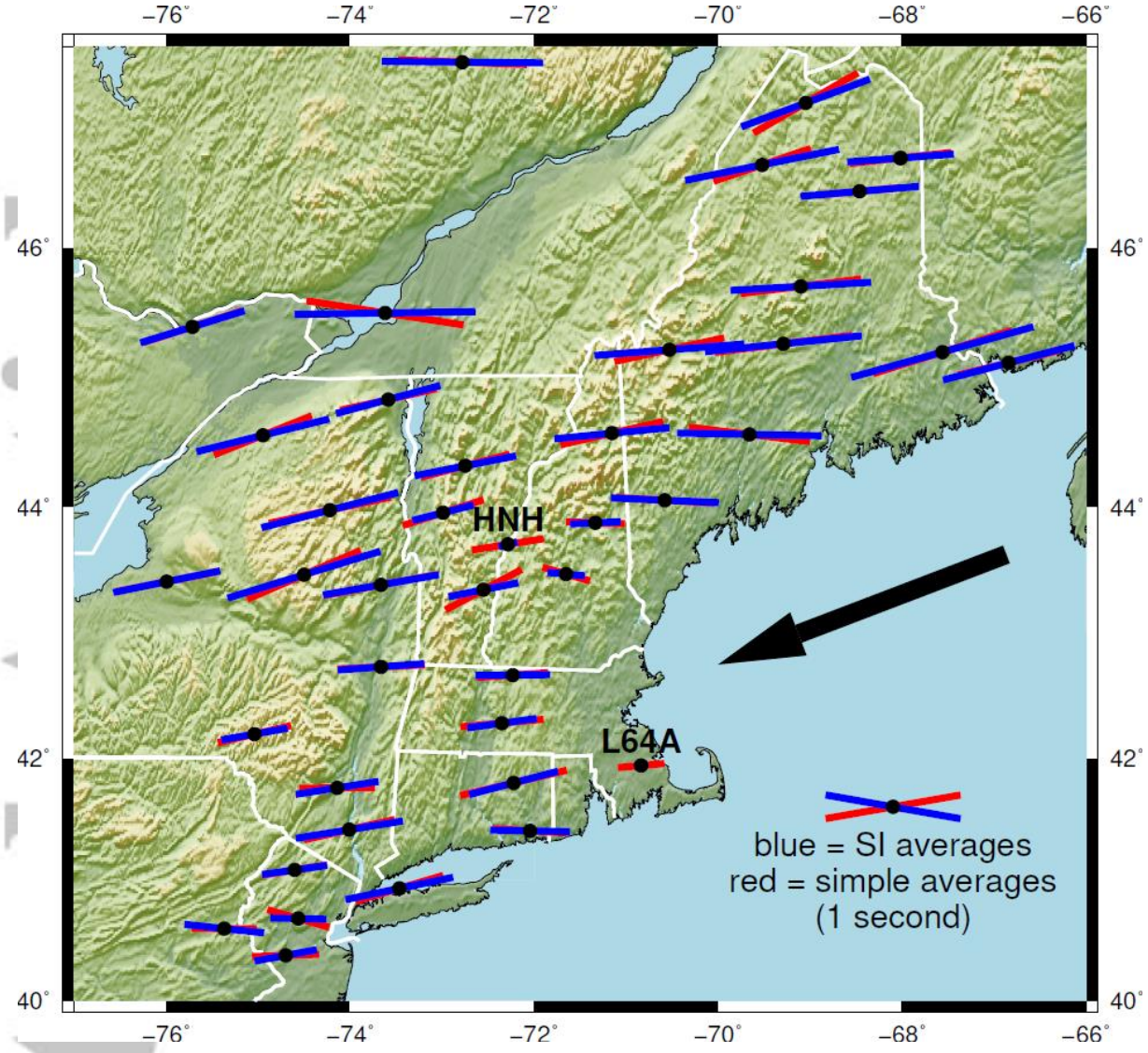


**Figure 4.** A map of averaged splitting parameters obtained by two methods; the blue bars indicate the values obtained by fitting SI observations, and the red bars indicate the values obtained by simple averaging of individual splitting values. The black dots indicate the location of 41 stations. The bars are scaled in proportion to the delay times and are oriented parallel to the estimated fast polarizations. The black arrow indicates the direction of regional absolute plate motion (approximately 249°) obtained from HS3-NUVEL-1A model.

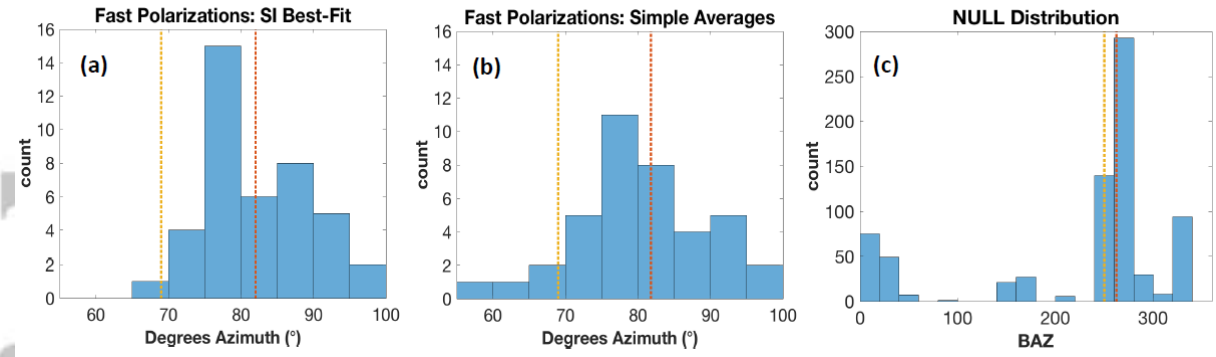


**Figure 5.** The distributions of averaged fast polarization orientations and the back azimuths that yielded NULL measurements. The red dashed lines indicate the mean fast axes orientations, and the yellow dashed lines indicate the regional absolute plate motion (249°) obtained from HS3-NUVEL1 plate model. (a) shows the best-fit values obtained using the SI technique (modulo 180°), (b) shows values obtained by simple averages of the split measurements, and (c) shows the back azimuths that yielded the NULL measurements.

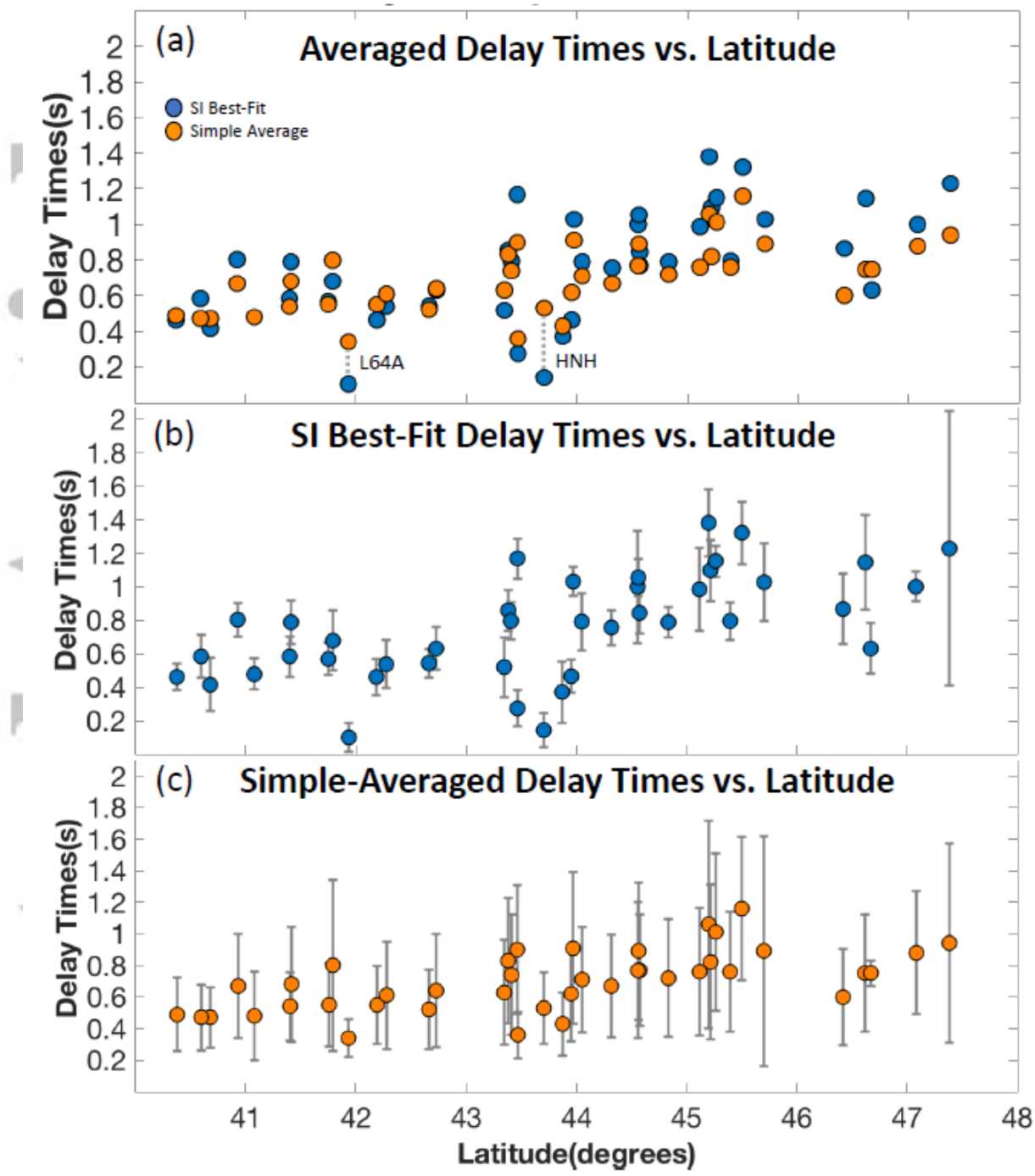


**Figure 6.** Regional trends of the delay times. (a) indicates the trends of averaged delay times plotted with respect to the latitude; the blue dots represent the values obtained by the SI technique, and the red dots represent the values obtained by simple averaging. (b) and (c) each indicate individual trends of delay times with error bars.

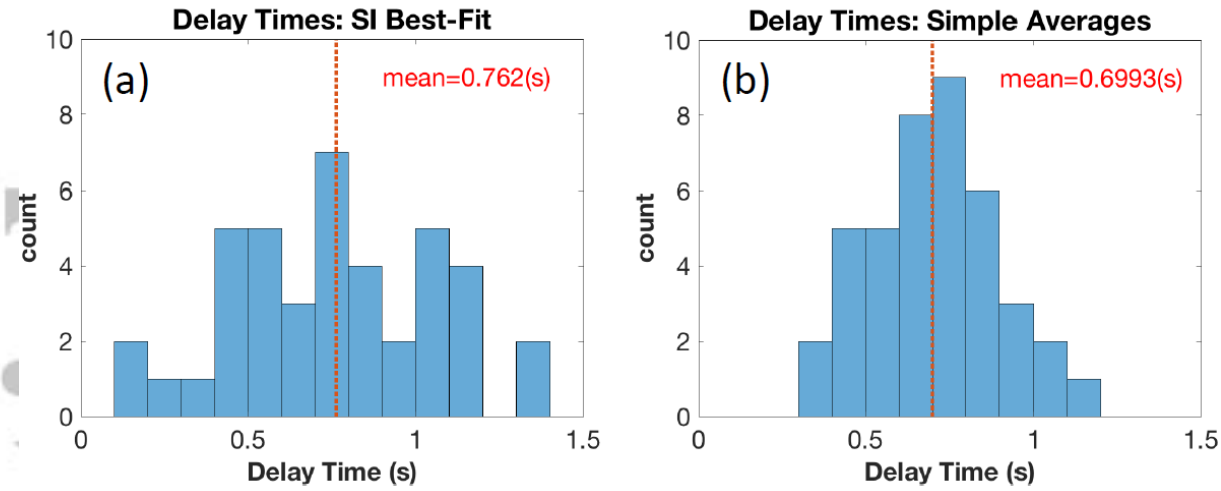


**Figure 7.** The distribution of station-averaged delay times obtained by both the SI technique and simple averaging. The red dashed lines indicate the mean delay times of each distributions. (a) indicates the delay times obtained by the SI technique, (b) indicates the delay times obtained by simple averaging.

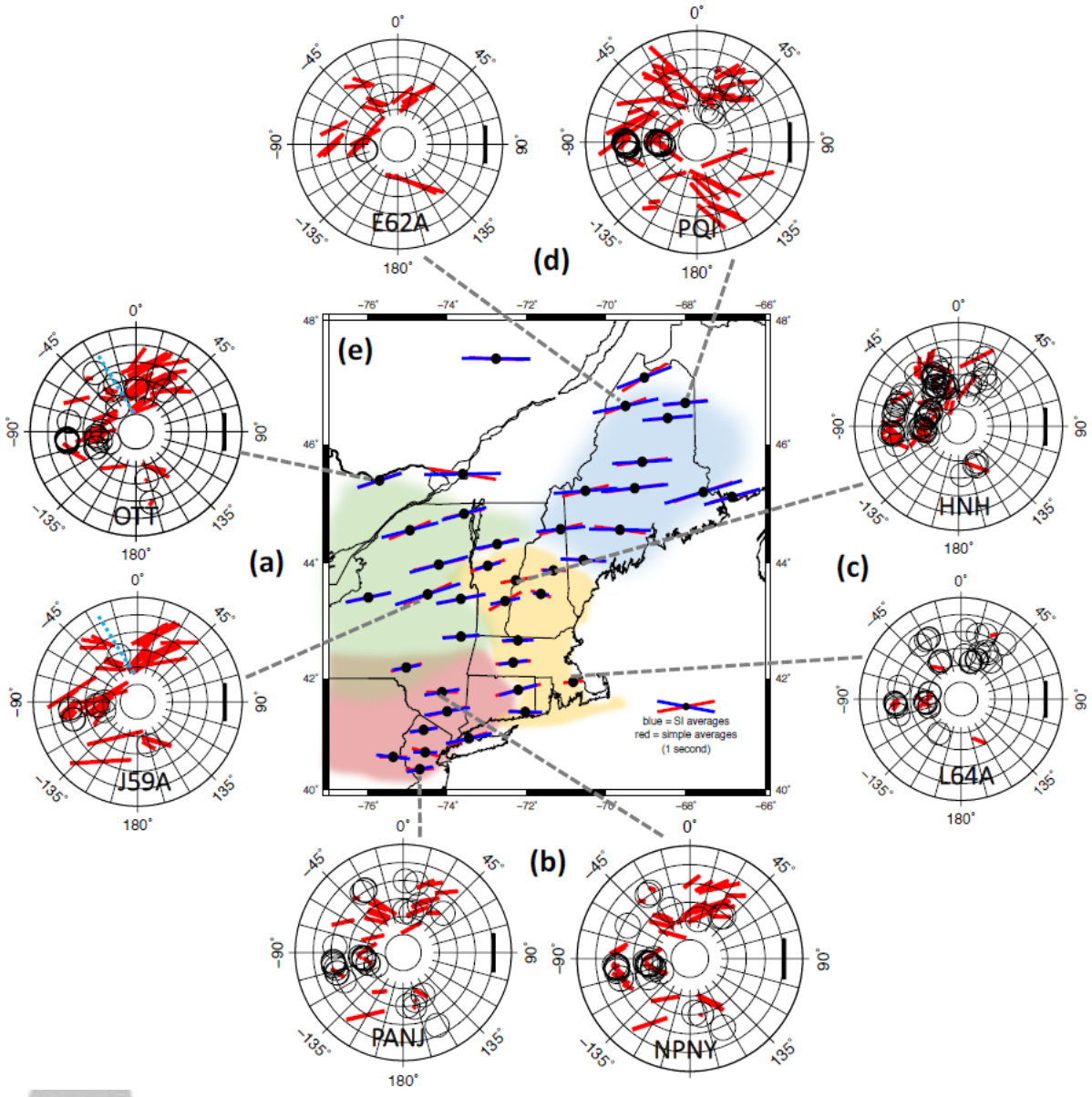


**Figure 8. Four** anisotropic domains grouped based on similar patterns of back azimuthal dependence, illustrated with representative examples of directional splitting variation diagrams. Sample stereonet plots are representative of (a) green domain, (b) red domain, (c) yellow domain, and (d) blue domain, respectively. The blue dashed lines in (a) for stations OTT and J59A mark the back azimuth at which the delay times drastically drop from the northeast to the northwest. The plots (a)-(d) follow the convention described in Figure 2c. (e) indicates the spatial distribution of the four domains, plotted with the pairs of averaged splitting parameters displayed in Figure 4.

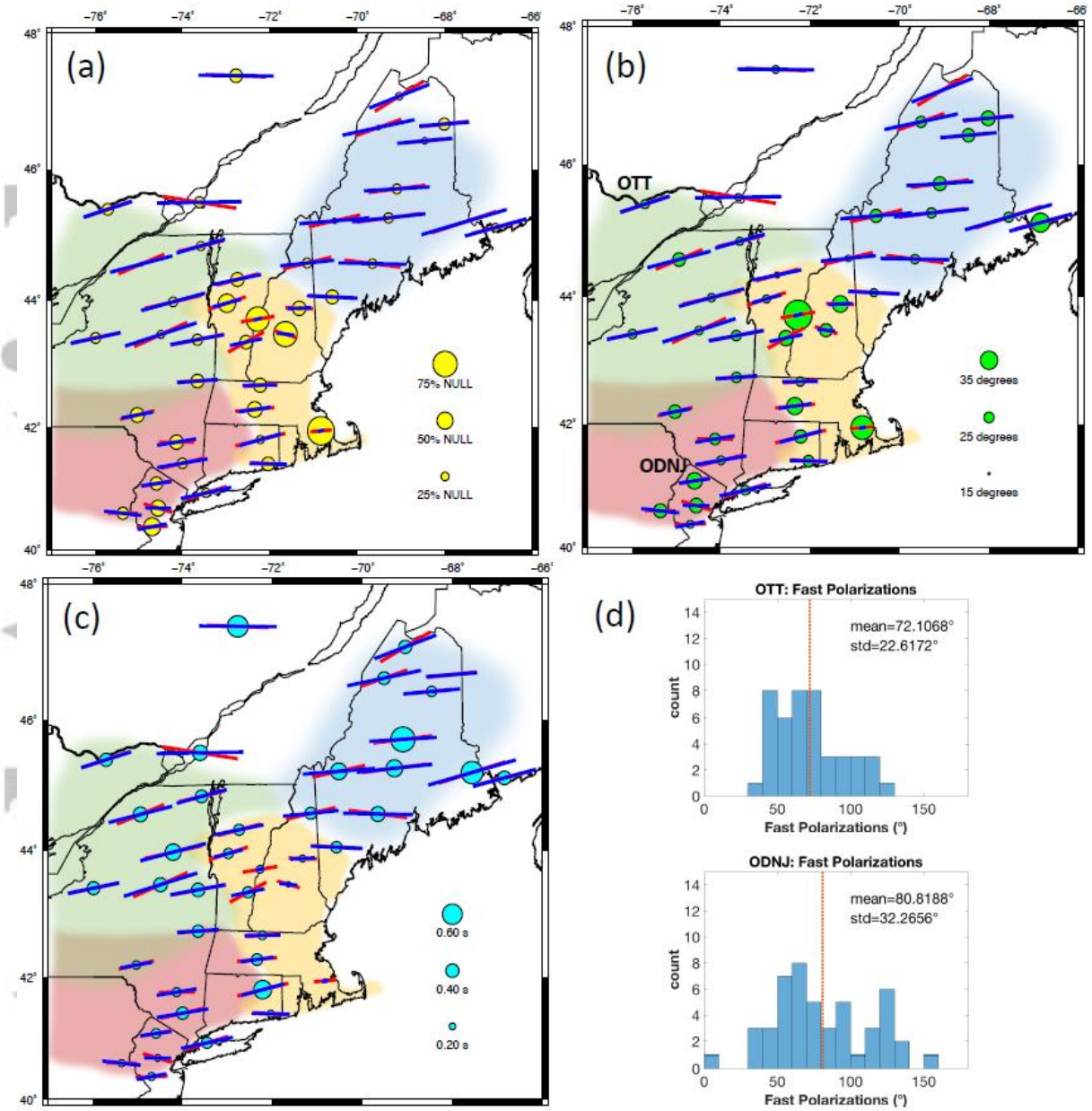


**Figure 9.** The regional distributions of selected statistical traits. (a) indicates the proportion of NULL measurements within the datasets of individual stations, (b) indicates the standard deviation of fast polarizations, and (c) indicates the standard deviation of delay times. (b) and (c) serve as the measures for the degree to which both splitting parameters vary. (d) shows examples of unimodal (top panel, station OTT) and bimodal (bottom panel, station ODNJ) distributions of fast polarization orientations.

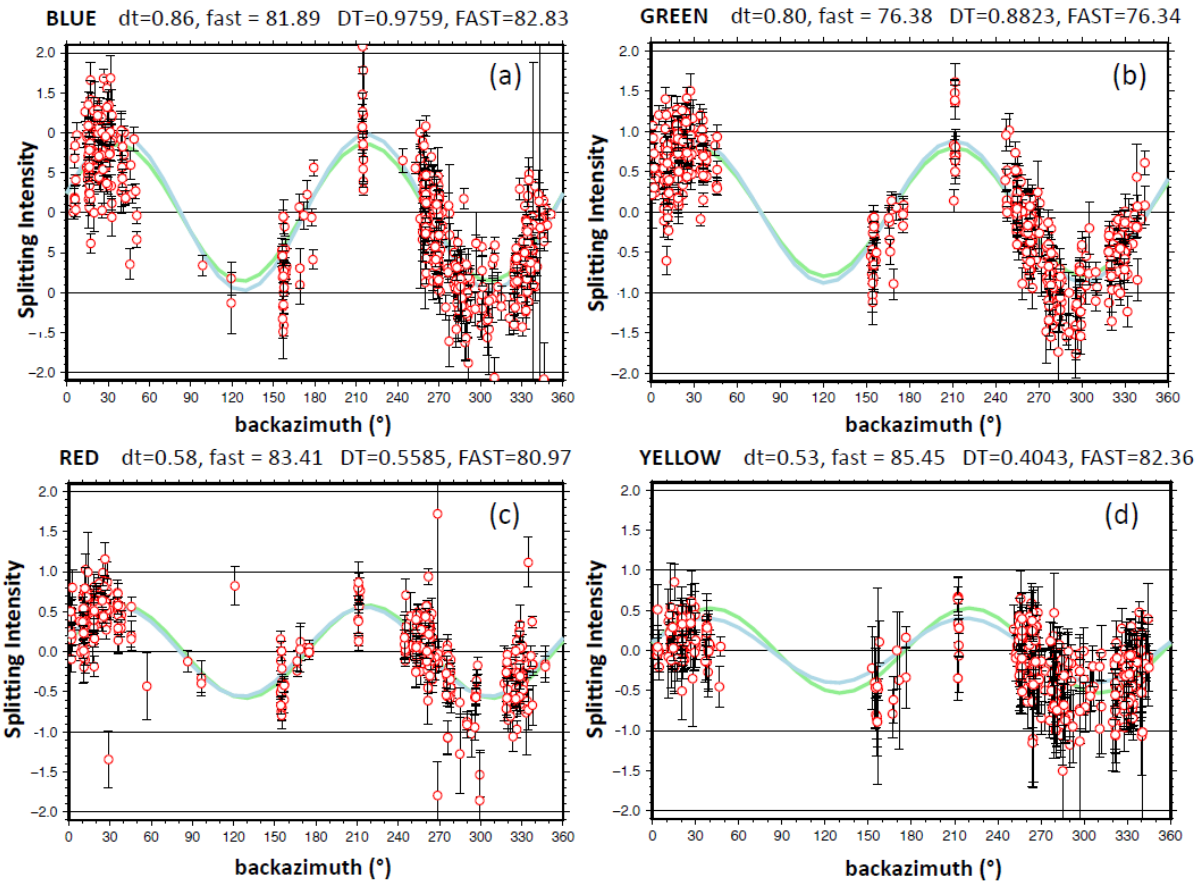


**Figure 10.** The sinusoid pattern of splitting intensity values fitted to all measurements within each domain. The blue lines in the SI plots are the best-fit curves determined by a least-squares fit for the parameters of function, $\delta t \times \sin [2(\varphi_o - \varphi)]$. The best-fit splitting parameters are indicated by delay time, DT, and fast polarization, FAST. The green lines are curves predicted based on the mean fast polarization and delay time of all split measurements within the specific domain. The averaged splitting parameters are indicated by delay time, dt, and fast polarization, fast. (a) indicates the blue domain, (b) indicates the green domain, (c) indicates the red domain, and (d) indicates the yellow domain.

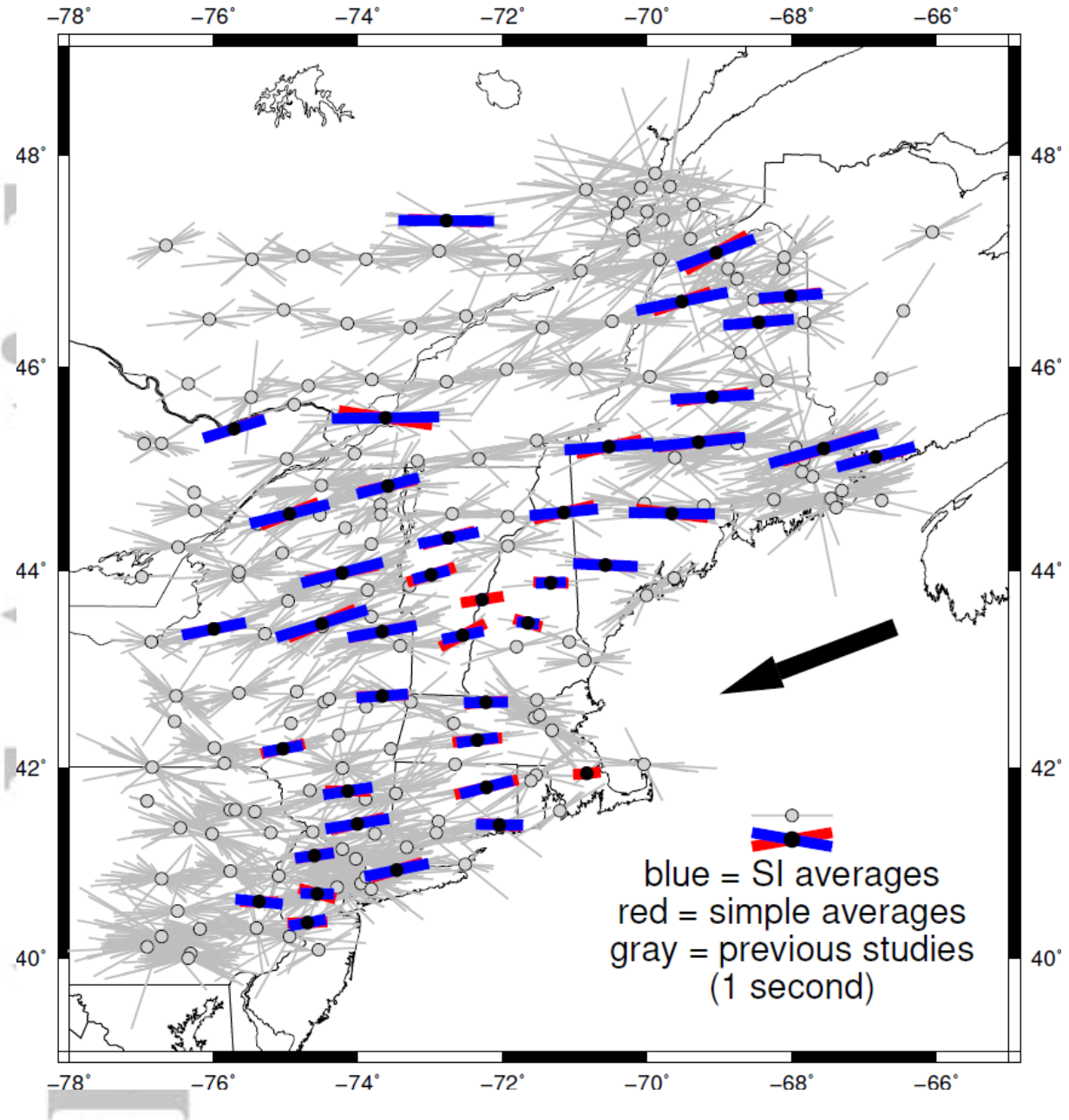


**Figure 11.** Comparison of our results with the results of previous studies done in this region. The gray bars indicate both single-event and station-averaged splitting parameters reported by the previous studies. The blue and red bars indicate our station-averaged splitting parameters, quantified by SI technique and simple-averaging, respectively. All bars are aligned to the orientations of fast polarization and are scaled proportional to the delay times. The black arrow indicates the direction of regional absolute plate motion (approximately 249°) obtained from HS3-NUVEL-1A model.

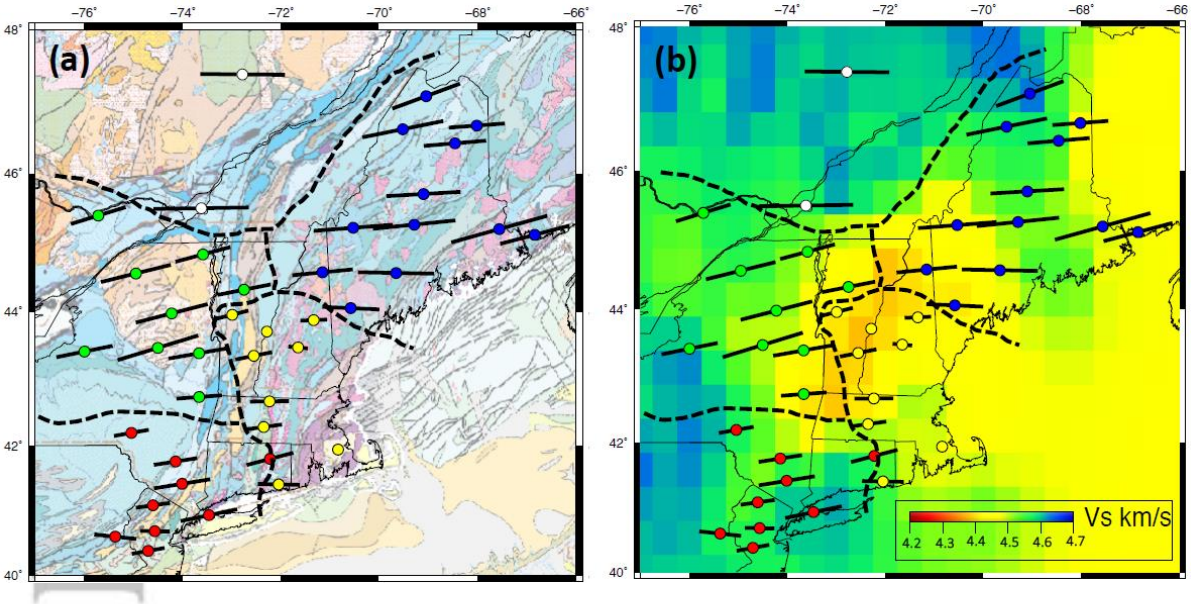


**Figure 12.** The comparison of anisotropic domains with (a) the surface geological map based on Garrity and Soller (2005) and (b) the shear wave velocity distribution of Shen & Ritzwoller (2016) at 90km depth. The four anisotropic domains are indicated by the different colors of the circles plotted at the location of each station. The black dashed lines indicate the inferred domain boundaries. The white stations are stations LATQ and MNTQ, which were deemed sufficiently different from the green and blue domains but were not sufficient to form a domain, due to the lack of station and sparsity. The black bars indicate the splitting parameters obtained by the SI technique.